

1 **The symmetrical pattern of base-pair substitution rates across the chromosome in**

2 ***Escherichia coli* has multiple causes**

3

4 Brittany A. Niccum¹, Heewook Lee², Wazim MohammedIsmail³, Haixu Tang³, and Patricia L. Foster^{1*}

5

6 ¹Department of Biology, Indiana University, Bloomington, IN, USA, 47405

7 ²School of Computer Science, Computational Biology Department, Carnegie-Mellon University

8 ³School of Informatics, Computing, and Engineering, Indiana University, Bloomington, IN, USA, 47405

9

10 *Corresponding Author:

11 Patricia L. Foster

12 Department of Biology

13 Jordan Hall 447E

14 1001 East Third Street

15 Indiana University

16 Bloomington, IN 47405

17 812-855-4084

18 plfoster@indiana.edu

19

20 Author email addresses:

21 Patricia L. Foster, plfoster@indiana.edu

22 Brittany A. Niccum, brittanyniccum@gmail.com

23 Heewook Lee, heewookl@cs.cmu.edu

24 Wazim MohammedIsmail, wazimoha@indiana.edu

25 Haixu Tang, hatang@indiana.edu

26 **Abstract**

27 Mutation accumulation experiments followed by whole-genome sequencing have revealed that for
28 several bacterial species the rate of base-pair substitutions is not constant across the chromosome but
29 varies in a wave-like pattern symmetrical about the origin of replication. The experiments reported
30 here demonstrate that in *Escherichia coli* several interacting factors determine the wave. Perturbing
31 replication timing, progression, or the structure of the terminus disrupts the pattern. Biases in error-
32 correction by proofreading and mismatch repair are major factors. The activities of the nucleoid
33 binding proteins, HU and Fis, are important, suggesting that mutation rates increase when highly
34 structured DNA is replicated. These factors should apply to most bacterial, and possibly eukaryotic,
35 genomes, and imply that different areas of the genome evolve at different rates.

36 **Keywords** *Escherichia coli*, mutation rate, mutation accumulation, whole genome sequencing,
37 mismatch repair, replication timing, nucleoid associated proteins, proofreading

38 **Author Summary**

39 In several species of bacteria the rate of single base-pair mutations is not constant across the genome,
40 but varies in a wave-like pattern that is symmetrical about the origin of replication. Using *Escherichia*
41 *coli* as our model system, we show that this wave is determined by the timing and progression of
42 replication and the structure of the region where replication terminates. In addition, biases in error
43 correction and the three dimensional structure of the DNA also are important. These factors should

44 apply to most bacterial, and possibly eukaryotic, genomes, and imply that different areas of the
45 genome evolve at different rates.

46 **Introduction**

47 Recent studies of mutations accumulated non-selectively across bacterial chromosomes have
48 revealed that rates of base-pair substitutions (BPSs) vary 2- to 4- fold in a wave like pattern that is
49 mirrored in the two independently replicating halves of the chromosome. Such symmetrical patterns
50 have been observed in mismatch-repair (MMR) defective strains of *Escherichia coli* (1), *Vibrio fischeri*,
51 *V. cholerae* (2-4), *Pseudomonas fluorescens* (5), and *P. aeruginosa* (6). Such variation in mutation rates
52 may affect the rate at which genes in different regions of the chromosome evolve, and may exert
53 selective pressure on gene placement. Yet the causes of this variation are not known.

54 The fidelity of DNA replication, which, in *E. coli*, is about 1 mistake in 1000 generations (7), is
55 determined by the intrinsic accuracy of the DNA polymerase and error correction by proofreading and
56 mismatch repair (reviewed in (8, 9). In *E. coli*, proofreading is performed by epsilon, a subunit of the
57 DNA polymerase III holoenzyme. If the polymerase inserts the incorrect base, epsilon's 5' to 3'
58 exonuclease activity degrades a few bases of the new strand and polymerase then re-synthesizes it.
59 The accuracy of DNA synthesis is improved about 4000-fold by proofreading (10). Mismatch repair is
60 performed by three proteins, MutS, MutL, and MutH. MutS recognizes a mismatch and recruits MutL.
61 Together they find a nearby GATC site in which, in *E. coli*, the A is methylated by the Dam methylase.
62 Because methylation lags behind replication, unmethylated As identify the "new", and presumably
63 error-containing, DNA strand. MutH is recruited by MutSL to the GATC site and activated to nick the
64 unmethylated DNA strand, which is then degraded past the mismatch by the concerted activity of the

65 UvrD helicase and one of four exonucleases. Pol III then re-synthesizes the strand. MMR improves the
66 accuracy of DNA replication 100 to 200 fold (11).

67 In our previous study of the BPS density pattern in MMR-defective *E. coli* (1), we correlated
68 mutation rates to the chromosomal sites that are affected by two nucleoid-associated proteins (NAPs),
69 HU and Fis. We suggested that when the replication fork encounters regions of the chromosome with
70 high superhelical density due to the binding of these NAPs, the mutation rate increases. An alternative
71 explanation ties mutation rates to replication timing (2, 3). An intriguing hypothesis is that mutation
72 rates vary in concert with fluctuations in dNTP concentration when the replication origin fires
73 repeatedly during rapid growth (2).

74 In the work presented here, we investigate further the causes of the wave-like pattern of BPS
75 rates. MMR-defective strains of *E. coli* additionally defective for other activities were used in mutation
76 accumulation (MA) experiments and the mutations identified by whole genome sequencing (WGS). We
77 also investigated the effects of different growth conditions on BPS rates. We conclude that the BPS
78 density pattern does not have a single cause, but is the result of several factors affecting DNA
79 replication, repair, and chromosome structure. In addition, we report that a MMR-defective *Bacillus*
80 *subtilis* also has a wave-like BPS density pattern that is symmetrical about the origin of replication.

81 **Results**

82 **The base-pair substitution (BPS) density pattern in mismatch repair-defective strains**

83 In a previous paper (1) we demonstrated that the density of BPS that accumulated across the
84 chromosome in a MMR-defective strain during an MA experiment fell into a wave-like pattern that was
85 symmetrical about the origin. We have since performed nine additional MA experiments with MMR
86 mutant strains, each experiment resulting in the accumulation of over 1000 BPSs, for a total of 30,061

87 BPSs (11). As shown in Figure 1A, the wave-like BPS density pattern was reproducible among the 10
88 experiments. Also as shown in Figure 1A, the mutational density pattern does not exactly match the
89 non-interacting chromosomal macrodomains (MCs) as defined by Valens et al, 2004 (12). In particular,
90 the wave pattern of BPSs is symmetrical about the origin whereas the Ori MC is not.

91 Following the analysis of Dillon et al, 2018 (2), we computed the wavelet coherence of the
92 collected MMR⁻ data taken in the clockwise and the counterclockwise directions around the
93 chromosome; supplementary Figure S1A shows that, except for some asymmetry at the midpoint, the
94 wave is symmetrical across the chromosome. The coherence is greatest between 800 to 1,600 Kb per
95 cycle (= 8 to 16 bins per cycle), which is a similar result to that found by Dillon et al, 2018 (2). We also
96 computed the wavelet coherence of the collected MMR⁻ data against each of the experimental results
97 discussed below, and these graphs are also given in the supplementary figures In the analyses below,
98 the combined data from the 10 experiments with MMR-defective strains are used as the standard to
99 which the results obtained in other genetic backgrounds are compared.

100 The spectrum of BPSs in the MMR-defective strains is dominated by A:T transitions at
101 5'NAC3'/3'NTG5' sites (11). To test if the mutational density pattern was simply due to the distribution
102 of these sites, we removed all the A:T transitions at 5'NAC3'/3'NTG5' sites from the data set. As shown
103 in supplementary Figures S5A, S6A, and Tables 1 and 2, although the mutation rate was reduced by
104 60% when these BPSs were removed, the remaining 12,542 BPSs fell into the same wave pattern. Thus,
105 the variation in BPS rates must be reflective of regions of the chromosome and not the distribution of
106 the hotspot DNA sequences.

107 **Transcription**

108 One obvious hypothesis is that the mutational density pattern reflects transcriptional patterns.
109 Mutation rates have been reported to be both increased (13) and decreased (14) by high levels of
110 transcription. In a previous paper (7) we reported that highly expressed genes had normal mutation
111 rates, a finding that was confirmed in a recent study using deep sequencing to detect mutations (15).
112 To determine if, nonetheless, transcription influences the wave pattern, we used RNA-Seq to
113 quantitate the RNA levels in a $\Delta mutL$ mutant strain in the lag, exponential, and stationary phases of
114 growth. These results should be representative of the cells in colonies during our MA experiments. We
115 then compared these results to the BPS density pattern by binning the RNA-Seq results into the same
116 bins as used for mutational data. As shown in Figure 1B and supplementary Figure S1B, there was no
117 similarity in the two data sets.

118 Because ribosomal operons are homologous, we could not call SNPs in these genes. The RNA
119 reads from the genes in ribosomal operons were also removed from the RNA-Seq data, but their
120 positions have been indicated in Figure 1B. Interestingly, bin 35, which includes the ribosomal *rrnG*
121 operon, has a high number of RNA reads even in the absence of reads from the *rrnG* genes. This high
122 level of expression is almost exclusively due to the *ssrA* gene, which encodes transfer-messenger RNA
123 (16), that is highly expressed under all three conditions (the RNA-Seq data will be further analyzed in a
124 subsequent paper). The BPS density pattern of several of the strains that will be discussed below tends
125 to reach a minimum in this general area, but it is as often at bin 33 as at bin 35. Given that the bin size
126 is 100 Kb, it seems unlikely that the high level of transcription level of *ssrA*, located in the middle of bin
127 35, is causing these patterns.

128 **Replication Initiation**

129 The BPS density pattern is centered on *oriC*, the origin of replication, and over many experiments
130 in different genetic backgrounds the pattern around the origin has proved to be stable. In both
131 replichores BPS rates decline to a minimum about 300 Kb from the origin and then increase until a
132 peak is reached about 900 Kb from the origin. Mutation rates then fall again and reach a minimum
133 about 3/5th of the distance along each replichore.

134 We tested whether replication initiation was responsible for the maintenance of this pattern by
135 performing MA experiments with strains with errant replication start sites. The *rnhA* gene encodes
136 RNase H1, which degrades RNA-DNA hybrids; in the absence of RNase H1, persistent R-loops can
137 initiate aberrant DNA replication and disrupt normal fork migration (17, 18). But an MA experiment
138 with a $\Delta rnhA \Delta mutL$ mutant strain showed no difference in the BPS density pattern from that of the
139 $\Delta mutL$ mutant strain (Figure 1C, Supplementary Figure S1C, Tables 1 and 2), indicating that aberrant
140 replication Initiation does not influence where mutations occur, at least not when a powerful *oriC* is
141 present.

142 To further test the influence of replication initiation on the mutational density pattern, we
143 performed MA experiments with strains that have a 5.1 Kb region containing *oriC* moved to the
144 midpoint of the right replichore, where it is called *oriZ* (19). These strains are derived from *E. coli* K12
145 strain AB1157, instead of MG1655 strain, the ancestor of our MA strains, and have a large inversion in
146 the right replichore that relieves the head-on collision between replication initiating at *oriZ* and
147 transcription of the *rrnCABE* operon (20). As a control we created an AB1157 $\Delta mutL$ mutant strain,
148 which had the similar wave-like BPS density pattern as our MMR⁻ strains, indicating that the pattern is
149 intrinsic to *E. coli* K12, not specific to sub-strain MG1655 (Supplementary Figures S5B, S6B, Tables 1
150 and 2). We performed MA experiments on $\Delta mutL$ derivatives of two additional strains: one with both

151 *oriZ* and *oriC* (WX320 $\Delta mutL$), and one with only *oriZ* (WX340 $\Delta mutL$). The strain that contained two
152 origins had a similar BPS density pattern as the MMR⁻ strains (Figure 1D, Supplementary Figure S1D,
153 Tables 1 and 2), suggesting that, under our conditions, firing of *oriZ* could not overcome the influence
154 of *oriC*. However, the strain containing only *oriZ* showed a decrease in BPS rate in the 200Kb-area
155 surrounding the new origin, similar to that normally observed about *oriC* (Figure 1E, Supplementary
156 Figure S1E, Tables 1 and 2).

157 **SeqA**

158 As mentioned above, in *E. coli* the adenines in GATC sites are methylated by the Dam
159 methylase. The SeqA protein binds to hemimethylated GATC sites, many of which are clustered around
160 OriC, and, by so doing, SeqA occludes the replication initiation protein, DnaA, hindering origin firing.
161 Sequestering of the origin persists for about one third of a generation; however, the mechanism of
162 relief is not clear. In the absence of SeqA, unregulated initiation presumably results in over-replication,
163 at least when cells are rapidly growing in rich medium (21). Downstream events, such as replication
164 fork collapse, add to the phenotypes of *seqA* mutant cells (22).

165 Loss of SeqA affects chromosomal structure in areas distant from OriC. By binding to
166 hemimethylated DNA, SeqA forms complexes behind the replication fork as it progresses around the
167 chromosome (21). In addition, SeqA binds to areas of the chromosome with closely spaced GATC sites,
168 as well as to particular genes regulated by GATC methylation (23). In the absence of SeqA the
169 superhelicity of the chromosome increases, the nucleoid condenses (24), and transcription is altered
170 (25).

171 To test whether SeqA affects the BPS density pattern, we performed an MA experiment with a
172 $\Delta mutL \Delta seqA$ mutant strain. As shown in Figure 1F, Supplementary Figure S1F, and Tables 1 and 2, loss

173 of SeqA somewhat amplified the BPS density pattern of the right replichore, but the pattern was still
174 highly correlated to that of right replichore of the MMR-defective strains. However, the pattern in the
175 left replichore was disrupted in the $\Delta seqA \Delta mutL$ mutant strain. Based on chromatin
176 immunoprecipitation analysis, this area of the left replichore is not targeted by SeqA to a greater
177 extent than the same area of the right replichore (23, 26), suggesting that the disruption of the
178 mutational pattern is not due to loss of binding by SeqA. As shown in Figure 1B, bins 44, 38, 37, and 35
179 contain a number of highly expressed genes; in addition, bins 42 and 35 contain highly transcribed
180 ribosomal RNA genes. Thus, we hypothesize that loss of SeqA makes the replication machinery
181 particularly susceptible to interference by transcription, disrupting the mutational pattern. If this
182 hypothesis is correct, the interference apparently makes replication more accurate, perhaps by slowing
183 the speed of DNA polymerase.

184 **Replication Fork Progression**

185 In a recent report, Dillon *et al.*, 2018 (2), hypothesized that the periodic variation in mutation
186 rates across the chromosome was tied to the timing of DNA replication. Cellular levels of dNTPs are
187 controlled by ribonucleotide reductase (RNR), the expression of which increases when the origin fires
188 (27, 28) }. In fast-growing bacteria in which new rounds of replication are initiated before cell division,
189 the levels of dNTPs should be high when each origin fires, but then fall as progression of the multiple
190 forks dilute the dNTPs. High levels of dNTPs are predicted to increase the probability of
191 misincorporation, and thus the mutation rate, whereas low levels of dNTPs should slow replication and
192 improve fidelity. This systematic fluctuation in dNTP levels could account for the pattern of mutational
193 density across the chromosome (2).

194 This hypothesis can be tested by examining the wave pattern from several experiments that we
195 have already published (11). The number of replicating chromosomes is a positive function of the cell's
196 growth rate (29). When $\Delta mutL$ or $\Delta mutS$ mutant strains were grown on glucose minimal medium,
197 which reduces the growth rate about 2-fold relative to growth on LB, the BPS density pattern became
198 chaotic (Figure 2A, Supplementary Figures S2A, S5C, S6C, Tables 1 and 2). Supplementing the minimal
199 medium with just enough LB to increase the growth rate to normal restored the wave-like BPS density
200 pattern (Figure 2B, Supplementary Figure S2B, Tables 1 and 2). Growing the cells on diluted LB, on
201 which the growth rate was the same as on minimal glucose medium, also preserved the wave-like BPS
202 density pattern (Figure 2C, Supplementary Figure S2C, Tables 1 and 2). When the cells were grown at a
203 lower temperature, which also reduced the growth rate 2-fold, the overall shape of the BPS density
204 pattern was retained, but the increases in BPS rates that normally peak at about 900 Kb from each side
205 of the origin were shifted about 200 Kb further from OriC (Figure 2D, Supplementary Figure S2D, Tables
206 1 and 2). In addition, the magnitude of the fluctuation of the BPS rate across the chromosome was
207 doubled. Thus, it appears that growth rate *per se* is not a major determinant of the BPS density
208 pattern, but other factors, such as the composition of the growth medium, are also important. For
209 example, the expressions and DNA binding characteristics of nucleoid associated proteins (NAPs) are
210 different under different growth conditions (30-32)

211 In *E. coli* growing aerobically dNTP levels are regulated by a Class Ia RNR encoded by the *nrdA*
212 and *nrdB* genes. Although most of this regulation appears to be due to DnaA interactions (28), the
213 NrdR repressor, which regulates a poorly expressed Class Ib RNR, also regulates *nrdAB* transcription;
214 loss of NrdR results in increased expression of RNR throughout the cell cycle (33). Increased RNR
215 should result in increased dNTP levels, and, indeed, the $\Delta nrdR \Delta mutL$ mutant strain had twice the

216 mutation rate as the MMR⁻ strains, as expected when dNTP levels are high (Supplementary Table S1).
217 As shown in Figure 2E, Supplementary Figure S2E, Tables 1 and 2, loss of NrdR did not change the basic
218 BPS density pattern, but the peak rate was shifted away from the origin about 200 Kb on each side.
219 This pattern was similar to that observed when cells were grown at low temperature, as described
220 above.

221 Replication fork progression is aided by the accessory replication helicase, Rep, and, in its
222 absence, the time required for chromosome duplication is doubled (34). Rep removes proteins bound
223 to the DNA in front of the fork (34, 35). While these nucleoproteins are primarily transcription
224 complexes (36, 37), Rep could also free the DNA of blocking NAPs. In addition, Rep aids in restarting
225 replication forks after they stall or collapse (38, 39). As shown in Figure 2F, Supplementary Figure S2F,
226 Tables 1 and 2, with the exception of a region close to the origin, loss of Rep disrupted the BPS density
227 pattern across the chromosome, suggesting that slowing or stalling the fork results in a distribution of
228 BPS that is essentially random.

229 **Replication Termination**

230 The results from almost all the strains tested show an increase in the BPS rate in the region
231 where replication terminates. The pattern of this increase varies somewhat among experiments.
232 Usually there are two unequal peaks, as shown in Figure 1A, but in some experiments these peaks are
233 better defined and of equal heights and occasionally there is just one peak. We do not know the source
234 of this variation, but suspect it is simply random noise.

235 Replication terminates approximately 180° from the origin in a 1200 Kb region bounded by
236 replication pause (Ter) sites; this region extends from bin 18 to bin 31 in our figures. The anti-helicase
237 Tus protein binds to the Ter sites and allows each replication fork to enter but not to exit, creating a

238 replication fork “trap”, within which the two forks fuse and the chromosome dimer is resolved (40). To
239 determine if the interaction of replication forks with Tus contributes to the increased mutation rate
240 within this region, we performed an MA experiment on a Δtus $\underline{\Delta mutL}$ mutant strain. As shown in Figure
241 2G, Supplementary Figure S2G, Tables 1 and 2, loss of Tus did not affect the BPS density pattern.

242 The Ter macrodomain (MD) extends from 1200 Kb to 2200 Kb (12), which is roughly from bin 20
243 to bin 28 in our figures. The structure of the Ter MD is maintained by the MatP protein, which binds to
244 23 *matS* sites within this region (41). In the absence of MatP, the Ter MD is disorganized, the DNA is
245 less compact, and the Ter MD segregates too early in the cell cycle and fails to localize properly at
246 midcell (41, 42). Because the mobility of the Ter MD is increased in the absence of MatP, DNA
247 interactions across MD barriers can occur in $\Delta matP$ mutant cells (41).

248 As shown in Figure 2H, Supplementary Figure S2H, Tables 1 and 2, loss of MatP caused a severe
249 disruption of the BPS density pattern. The mutation rates in the Ter MD were depressed whereas new
250 peaks appeared on either side of the Ter MD in the Right and Left MDs. Interestingly, the BPS pattern
251 near the origin was maintained in the right but not in the left replichore.

252 **Recombination and the SOS response**

253 Homologous recombination is intimately connected to replication. As replication proceeds,
254 various blocks, such as DNA lesions, transcription complexes, and DNA secondary structures, can cause
255 the replisome to pause and to eventually disassemble. This potentially lethal event is prevented by
256 recombination, which can repair and restart the replisome (43). In addition, the termination region is
257 subject to hyperrecombination (44, 45) particularly in the region bounded by TerA and TerB (our bins
258 21 to 24), named the terminal recombination zone (TRZ) (46, 47).

259 Elimination of *E. coli*'s major recombinase, RecA, had a modest effect on the mutational density
260 pattern. As shown in Figure 3A, Supplementary Figures S3A, S5D, S6D, Tables 1 and 2, in the *recA mutL*
261 and *recA mutS* mutant strains, BPS rates declined in bins 21 to 25, corresponding fairly well to the TRZ
262 described above. However, the hyperrecombination within the TRZ is dependent on the recombination
263 pathway defined by participation of the RecBCD complex. When we eliminated RecB, the mutational
264 density pattern did not phenocopy that seen when RecA was absent (Supplementary Figures S5E, S6E,
265 Tables 1 and 2). Either our protocol is not sensitive enough to detect an effect of loss of RecB, or
266 another recombination pathway, *e.g.* RecFOR (48), is sufficient to maintain the mutation rate in the
267 region.

268 In addition to its role in recombination, RecA is also a master regulator of the SOS response to
269 DNA damage, which includes the induction of two error-prone DNA polymerases, DNA Pol IV and V. To
270 test whether these polymerases are involved in determining the BPS density pattern, we performed an
271 MA experiment on a strain deleted for the genes that encode Pol IV, *dinB*, and PolV, *umuDC*. As shown
272 in Figure 3B, Supplementary Figure S3B, Tables 1 and 2, the BPS density pattern in the *mutL dinB*
273 *umuDC* mutant strain was not significantly different than the MMR⁻ pattern. The genes of the SOS
274 response are repressed by the LexA protein; the *lexA3* allele encodes a super-repressor LexA protein
275 that prevents the SOS genes from being induced (49). When this allele was present the BPS density
276 pattern was also unaffected (Figure 3C, Supplementary Figure S3C, Tables 1 and 2). Thus, the SOS
277 response appears to play no role in determining the pattern of BPSs across the chromosome.

278 **Nucleoid Associated Proteins**

279 In a previous report (1), we found that the BPS density pattern of a $\Delta mutL$ strain was correlated
280 with the density of genes activated by the HU protein and repressed by the Fis protein. Combining

281 these two factors in a linear correlation model accounted for 33% of the variation in the mutational
282 data. HU constrains supercoils and compacts the DNA into nucleosome-like particles; Fis also
283 constrains supercoils but, in addition, bends the DNA (31). While both of these NAPs affect
284 transcription, the general lack of correlation of the BPS rate with transcriptional levels (7); also see
285 above) led us to hypothesize that mutation rates across the chromosome were correlated not with
286 transcription *per se*, but with areas of high DNA structure (1). To further test this hypothesis we
287 preformed MA experiments with MMR⁻ mutant strains also defective for each of a number of NAPs.

288 HU exists as a dimer of its two subunits, HU α and HU β , encoded by the paralogous genes *hupA*
289 and *hupB*, respectively, in the three possible configurations. While loss of both subunits confers a
290 severe growth defect, loss of only one has little consequence during a normal growth cycle, suggesting
291 they can substitute for each other. HU $\alpha\beta$ is the dominant form over most of the cell cycle, but
292 significant amounts of HU α_2 are found during lag phase and early exponential phase, and HU β_2 is
293 prominent in stationary phase (30). Chromatin immunoprecipitation sequencing (ChIP-Seq) results
294 revealed that HU binds non-specifically to the chromosome and the DNA binding patterns of the three
295 dimers appear to be identical (50).

296 We performed MA experiments with both $\Delta hupA \Delta mutL$ and $\Delta hupB \Delta mutL$ mutant strains. As
297 shown in Figures 3D, 3E, Supplementary Figures S3D, S3E, Tables 1 and 2, although loss of *hupB*
298 appeared to affect the BPS density pattern, the differences from the MMR⁻ pattern were not
299 significant. However, loss of *hupA* depressed mutation rates across the chromosome, particularly in the
300 terminus region, while creating new peaks on either side of the Ter MD.

301 Fis has many binding sites across the chromosome, but, based on data at RegulonDB, SOBETZKO *et*
302 *al.* (2012) (51) reported more Fis binding sites in the origin region. However both Chromatin

303 immunoprecipitation plus microarray analysis (ChIP-chip) and ChIP-Seq studies found the density of Fis
304 binding to be more-or-less constant across the chromosome (32, 52). Loss of Fis in both $\Delta fis \Delta mutL$ and
305 $\Delta fis \Delta mutS$ mutant strains tended to flatten the BPS density pattern across the chromosome except in
306 the region around the origin (Figure 3F, Supplementary Figures S3F, S5F, S6F, Tables 1 and 2).

307 The NAP HNS binds to DNA at its high-affinity binding sites and then spreads by oligomerization
308 along A:T rich regions of DNA. Bridging between HNS-DNA complexes condenses the DNA into a few
309 clusters per chromosome (53-55). However, as shown in Figure 3G, Supplementary Figure S3G, Tables
310 1 and 2), loss of HNS had little effect on the BPS density pattern, and, thus, the long-range structures
311 produced by HNS appear not to affect BPS rates.

312 The DPS protein accumulates in stationary phase cells, condenses the nucleoid into a crystalline-
313 like state, and protects the DNA from oxidative and other damage (56). Despite this radical physical
314 change, loss of DPS had little effect on the BPS density pattern Figure 3H, Supplementary Figure S3H,
315 Tables 1 and 2). Of course, we do not know the degree to which cells in stationary phase contribute to
316 the BPS rates under our experimental conditions.

317 **Proofreading**

318 As mentioned above, epsilon is the proofreading subunit of the DNA polymerase III holoenzyme.
319 The *mutD5* allele encodes an epsilon protein that is inactive for proofreading, and strains carrying this
320 allele have a mutation rate 4000-fold greater than that of wild-type strains, and 35-fold greater than
321 that of MMR-defective strains (10). As shown in Figure 4A, Supplementary Figure S4A, Tables 1 and 2,
322 when proofreading was inactive but MMR was active, the BPS density pattern was less dramatic than
323 when MMR was inactive and proofreading was active; but, nonetheless, the wave pattern was basically
324 the same. When both MMR and proofreading were inactive, which reveals the mutations solely due to

325 replication errors, the BPS density pattern was nearly flat but around the origin it retained significant
326 correlations to the patterns of both the MMR-defective and *mutD5* mutant strains (Figure 4B,
327 Supplementary Figure S4B, Tables 1 and 2). Thus, the pattern of BPS on both sides of the origin appears
328 to be established by replication errors and then elsewhere across the chromosome the density pattern
329 is largely due to differential error-correction by both proofreading and MMR.

330 **Wild-type**

331 The mutational density wave patterns evident in our data, and in data from other bacteria (2, 3),
332 were obtained when MMR was inactive. Thus, the question arises: does the pattern appear in wild-
333 type strains? It is difficult to answer this question because mutation rates in wild-type strains are so
334 low (in *E. coli*, 120-fold lower than that of MMR-defective strains (7, 11) that enormous experiments
335 would have to be conducted in order to accumulate enough mutations to approach statistical
336 confidence. In a recent study we compared the mutation rates and spectra of a number of *E. coli*
337 strains defective in various DNA repair activities; of these, the results from seven strains were
338 indistinguishable from those of the wild-type parent (57). By combining the mutations from these
339 strains, we achieved 1933 BPSs (11), enough to expect to see a wave pattern if it existed. As is evident
340 in Figures 4C, 4D, Supplementary Figures S4C, S4D, Tables 1 and 2, these BPSs did not create fall into a
341 recognizable pattern. Indeed, the pattern from the wild-type strains appears to be random; the
342 variance to mean ratio of the binned mutations is 1.4, indicating the values are not disperse, and the
343 MatLab “runstest”, a test for runs, returns a P value of 0.58, also indicating that the bin values are
344 random. In the wild-type strain both MMR and proofreading are active, and, while these two activities
345 have similar correction biases (Figure 4A), proofreading is much more powerful, producing the pattern
346 seen in the MMR-defective strains. Although we cannot conclude that the mutational density pattern

347 in the wild-type strain is other than random, it does have similarity to both the patterns seen in the
348 MMR-defective strains and in the *mutD5* mutant strain, particularly around the terminus (Figures 4C,
349 4D, Supplementary Figures S4C, S4D and Tables 1 and 2).

350 ***Bacillus subtilis***

351 In additional to *E. coli* strains, symmetrical mutational density patterns have been demonstrated
352 in MMR- derivatives of *Vibrio fischeri*, *V. cholera* (2-4), *Pseudomonas fluorescens* (5), and *P. aeruginosa*
353 (6). Here we add *Bacillus subtilis* to this list. As shown in Figure 4E, Supplementary Figure S4E, Tables 1
354 and 2, the BPS mutation rates in a *B. subtilis mutS::Tn10* mutant strain fell into a wave like pattern that
355 was symmetrical about the origin. Although similar in shape, the pattern was significantly different
356 from that of *E. coli* (Figure 4E, Supplementary Figure S4F, Tables 1 and 2). However, as in *E. coli*, the
357 BPS rate appeared to increase in the terminus region, which in *B. subtilis* is not 180° from the origin
358 and corresponds to bins 20-24 in Figure 4E.

359 **Discussion**

360 In this report we have examined a number of factors that could be responsible for establishment
361 and maintenance of the symmetrical wave-like BPS density pattern across the chromosome. In broad
362 terms these factors were: transcription; DNA replication initiation, progression, and termination;
363 recombination and the SOS response to DNA damage; the binding of nucleoid-associated proteins;
364 and, error-correction by MMR and proofreading. As discussed above, we found that transcription and
365 the SOS response had little effect, and the effect of recombination was modest and confined to the
366 terminal region. We discuss the more significant, factors in greater detail here.

367 **DNA replication initiation, progression, and termination**

368 Providing additional replication origins, either by eliminating RNase H1 or by inserting an ectopic
369 *oriC* (*oriZ*), did not disrupt the wave (Figure 1C and 1D). However, when *oriZ* was the only origin of
370 replication, the region of depressed BPS rate that surrounds *oriC* when it is in the normal position was
371 re-established about the new origin (Figure 1E). Note that only 5.1 Kb of DNA containing *oriC* was
372 relocated (19), whereas the region of reduced mutation rate is about 200 Kb; thus, the mutation rate is
373 not determined just by the DNA sequence surrounding the origin. We hypothesize that the process of
374 replication initiation protects the DNA from damage and/or newly established replication forks have a
375 low error-rate. In addition, the BPS mutation rate was increased for about 1000 Kb (10 bins) on either
376 side the new origin so that it resembled the same region about the normal origin. The size of this area
377 is close to the same size detected as “interacting zones” around *oriZ* (58). However, the mutational
378 density pattern across the rest of the chromosome did not re-establish itself to be symmetrical about
379 *oriZ*, but remained symmetrical about the absent *oriC*. Thus, other factors must be important at distant
380 regions. We can also conclude that the overall structure of the BPS pattern across the chromosome is
381 not determined by active replication initiation *per se*, but may have evolved in response to replication
382 initiation.

383 Both *V. fischeri* and *V. cholera* have multiple circular chromosomes of different sizes; by
384 comparing the mutational density patterns of these chromosomes, Dillon et al, 2018 (2) identified the
385 timing of replication as a significant determinant of the mutational density patterns. As mentioned
386 above, they suggested that the pattern could be the result of variations in the levels of dNTPs as origins
387 fire during rapid growth. Our results provide partial support for this hypothesis, but also indicate that
388 growth on rich medium, not growth rate *per se*, is a significant determinant of the mutational density
389 pattern, possibly because of effects on the expression and DNA binding of HU and Fis (see below). Our

390 results with a $\Delta nrdR$ mutant strain (Figure 2E) also show that dNTP levels are important, but, again,
391 other factors are driving the overall wave pattern. In addition, the results with the Δrep mutant strain
392 (Figure 2F) indicate that radically interrupting the progression of the replication fork disrupts the
393 mutational density pattern.

394 After declining to a local minimum about $3/5^{\text{th}}$ of the distance along each replicore, mutation
395 rates rise in the terminus region (Figure 1A). We originally hypothesized that this increase was due to
396 collisions of the replication complexes with the Tus anti-helicase, most of which would take place in
397 the region between bins 18 and 31 (1). However, elimination of Tus had no effect on the wave pattern
398 (Figure 2G, Supplementary Figure S2G), refuting this hypothesis. But, eliminating MatP, the protein
399 that maintains the structure of the Ter MD, reduced mutation rates in the Ter MD, suggesting that
400 replication of highly structured DNA is error-prone (Figure 2H, Supplementary Figure S2H).
401 Interestingly, in $\Delta matP$ mutant cells mutation rates increased in the Right and Left MCs, suggesting
402 that in the absence of MatP, these adjacent regions of DNA gained structure. The mechanism by which
403 MatP structures the Ter MC is not clear (59, 60), but it probably involves supercoils which, when
404 unconstrained, could migrate into adjacent areas. However, two studies have found that loss of MatP
405 increases the mobility and long-range interactions of adjacent DNA (41, 61). Resolution of these
406 conflicts will require further experimentation.

407 *Nucleoid-associated proteins*

408 Our previous results predicted that the NAPs HU and Fis should play a role in establishing or
409 maintaining the wave-pattern of BPS, but HNS should not (1). The results presented here confirmed
410 that prediction. In addition, we also found that Dps had no effect on the BPS density pattern. Because
411 the NAPs affect gene expression in various ways, we cannot conclude that DNA binding by the NAPs

412 themselves is responsible for the mutational pattern. And, indeed, we found no significant positive
413 correlations between the BPS pattern and published binding sites of the NAPs, although the location of
414 the binding sites themselves vary widely among published results (e.g. see (32, 50) and the data in
415 RegulonDB (62). Nonetheless, we favor the hypothesis that structuring of the DNA by the NAPs,
416 directly or indirectly, contributes to the BPS pattern.

417 The local effect of HU binding is to bend the DNA, but dimer-dimer interactions produce higher-
418 order HU-DNA complexes that can constrain negative supercoils (63, 64). The analysis of the effect of
419 HU on the mutational density pattern is also complicated by the variation in the cellular concentrations
420 of the three forms with growth cycle (30). Although the two subunits can compensated for each other
421 for viability, the affinities of three forms of HU for various DNA structures (linear, nicked, and gapped)
422 differ (65). Both HU α_2 and HU $\alpha\beta$ can constrain supercoils, but HU β_2 apparently cannot, at least *in vitro*
423 (30). Since HU β is not stable (66), the phenotype of a $\Delta hupA$ mutant strain may simply be that of low
424 cellular HU concentration.

425 While loss of HU β had little effect on the mutational density pattern (Figure 3D, Supplementary
426 Figure S3D), loss of HU α reduced the overall BPS rate by 33% and also changed the pattern (Figure 3E,
427 A Supplementary Figure S3E). In the $\Delta hupA \Delta mutL$ mutant strain, mutation rates were low in the
428 terminus region but elevated in the Right and Left MCs, very similar to the pattern seen in the $\Delta matP$
429 $\Delta mutL$ mutant strain (Figure 2H). The low mutation rate in the Ter MD corresponds well with the
430 density of genes activated in wild-type cells but not in HU-deleted cells (67). HU regulates transcription
431 by modifying the DNA superhelical density, suggesting that, like MatP, HU increases the structure of
432 the DNA in the terminal region, causing DNA replication to become error-prone.

433 The mutational pattern in the $\Delta hupA \Delta mutL$ mutant strain is also similar to that of the $\Delta recA$
434 $\Delta mutL$ strain (Figure 3A). An mutation accumulation experiment with a $\Delta hupA \Delta recA \Delta mutL$ mutant
435 strain resulted in a pattern similar to both single mutant strains, and so was not informative (data not
436 shown).

437 Fis is a major transcriptional regulator, either activating or repressing, directly or indirectly,
438 nearly a thousand genes (52). At some promoters Fis acts as a classic transcriptional regulator by
439 interacting with RNA polymerase, but at other promoters Fis affects gene expression by altering the
440 DNA superhelical density (68). The Fis DNA binding sequence is degenerate and the estimated number
441 of binding sites identified by sequence analysis across the genome varies widely among studies. The
442 results of ChIP analyses also vary: the number of DNA regions associated with Fis in different studies
443 ranges from 200 to 1500, which may reflect the effects of different growth conditions (32, 52, 69).

444 The loss of Fis nearly doubled the overall BPS rate, but flattened the wave pattern outside of the
445 origin region (Figure 3F, Supplementary Figures S5F, S6F). As mentioned above, the mutational density
446 pattern MMR⁻ strains is correlated to the density of genes activated in a Δfis mutant strain as reported
447 by Blot *et al*, 2006 (70). This correlation is particularly strong in bins 14 to 33 ($\rho = 0.62$, $P = 0.003$),
448 which corresponds to the area flattened in the $\Delta fis \Delta mutL$ and $\Delta fis \Delta mutS$ mutant strains. However, no
449 correlation exists between our mutational data and genes found to be responsive to Fis in a recent
450 study (32). Clearly more studies are needed to resolve these conflicts.

451 *Error-correction*

452 Assuming that the BPS recovered from the $mutD5 \Delta mutL$ mutant strain are due to intrinsic errors
453 made by DNA polymerase, we conclude that the polymerase is accurate close to the origin, then
454 becomes increasingly less accurate as replication proceeds to about 1/3 of the replichore, at which

455 point accuracy increases again (Figure 4B). The mutational pattern in the MMR-defective strains must
456 reflect the biased ability of proofreader to correct these polymerase errors. Thus, proofreading is
457 effective close to the origin, but then declines for about 1/3 of the replicore, increases in the Right
458 and Left MCs, but declines again in the terminus region (Figures 1A, 4B). Mutations in the *mutD5*
459 mutant strain are due to the failure of MMR to correct the polymerase errors that survive in the
460 absence of proofreading. Since the mutational pattern in the *mutD5* mutant strain mimics that of the
461 MMR-defective strains (Figure 4A, Supplementary Figure S4A, Tables 1 and 2), error correction by
462 MMR, although much less powerful, apparently has the same biases as error correction by
463 proofreader.

464 Given the above considerations, we would expect the mutational density pattern in the wild-type
465 parental strain to mimic that of the MMR-defective strains. However, the nearly 2000 BPS accumulated
466 in eight strains with wild-type mutational phenotypes appear randomly distributed across the
467 chromosome (Figures 4C, 4D). One explanation for this discrepancy is that when both proofreading and
468 MMR are active, the mutation rate is reduced to the point that other, weaker DNA repair and
469 mutagenic activities obscure the underlying pattern. Although not significantly correlated, the wild-
470 type BPS pattern is similar to the MMR⁻ pattern, particularly around the terminus, supporting this
471 hypothesis. Alternatively, although the eight strains that we combined to produce 2000 BPS have the
472 same mutation rates, they may have different wave patterns that tend to negate each other and
473 obscure the underlying wild-type pattern.

474 **Conclusions**

475 By applying mutation accumulation followed by whole-genome sequencing to bacterial strains mutant
476 in various activities we have determined that the most important factors determining the symmetrical

477 pattern of BPS rates across the chromosome are: the initiation, progression, and termination of DNA
478 replication, replication error-correction, and chromosome structure. Because of the conservation of
479 these factors, our results should apply to most bacteria, and possibly eukaryotes, and imply that
480 different regions of the genome evolve at different rates.

481 **Methods**

482 **Bacterial Strains and Media**

483 The strains used in this study are listed in Supplementary Table S1 and the methods of their
484 construction are in Supplementary file: Materials and Methods. Standard media and antibiotics were
485 used (see Supplementary file: Material and Methods).

486 **Mutation accumulation experiments**

487 The complete MA procedure has been extensively described (7, 11, 57). Details are given in the
488 Supplementary file: Material and Methods

489 **Genomic DNA Preparation, Library construction, Sequencing, and Sequence Analysis**

490 Details are given in the Supplementary file: Material and Methods.

491 **RNA sequencing**

492 The *E. coli* strain PFM144, which is PFM2 $\Delta mutL$ (11), was grown in LB and aliquots collected
493 during lag (OD = 0.022), log (OD = 0.3), and stationary (OD = 1.5) phase. The number of cells collected
494 was kept constant for each growth phase. Total RNA was extracted, DNA and rRNA were removed, and
495 libraries constructed and sequenced as detailed in the Supplementary file: Material and Methods.
496 Three biological triplicates were prepared for each growth phase.
497 A complete analysis of the RNA-Seq results will be the subject of a subsequent report. For this report
498 the numbers of RNA-Seq reads for each condition were first normalized to the number of reads

499 mapped to the gene *hold*, which was determined by rtPCR to be expressed at the same level in all
500 phases of growth. The means of the normalized RNA reads from the triplicates were then binned into
501 the same bins used for the mutational analysis. A fourth-order Daubechies wavelet transform was
502 performed on the binned RNA-Seq reads as described for the mutational data (1).

503 **Statistical Analysis**

504 To obtain the BPS density patterns, the numbers of BPSs were binned into 46 bins, each 100 Kb long, as
505 described (1). A fourth-order Daubechies wavelet transform was performed on the binned mutation
506 data as described (1). For presentation in the figures, these results were converted into rates by
507 dividing the number of BPS by the appropriate number of generations. Pearson's product-moment
508 correlation coefficient, ρ , was used to evaluate the correlations between the binned BPS data (Table
509 1). Spearman's nonparametric correlation coefficient was also computed for a few data sets, but gave
510 similar results. To account for multiple comparisons, p values were adjusted using the Benjamini-
511 Hochberg method (71) with the false discovery rate set at 25%, implemented with the MatLab R2018a
512 "mafdr" command. Because comparisons using the data from the same strain are not independent,
513 this adjustment was made separately for each column in Tables 1 and 2.

514 To further compare the BPS density patterns between two data sets, wavelet coherence was calculated
515 and plotted using the MatLab R2018a "wcoherence" command. While the Daubechies wavelet
516 provides a good visual representation of the binned data, it is not continuous and thus not easily
517 adapted for wavelet coherence analysis. The MatLab program first converts the binned data to Morlet
518 wavelets and then computes the coherence between two of these wavelets. We chose to analyze the
519 data with wavelet coherence because it gives a measure of the correlation between the signals
520 (displayed as colors in the figures) (72, 73). In addition, the MatLab wavelet coherence plot indicates,

521 as a dashed curve, the ‘cone of influence’ within which results are free of artifactual edge effects (72).
522 The relative phase-lag between the two signals is indicated by small arrows: arrows pointing right
523 indicate in-phase, arrows pointing left indicate 180° out-of-phase, and arrows pointing in other
524 directions indicate the various degrees in between. Because the MatLab program assumes a
525 frequency-time series, the X axis of the plot is cycles/sample and the Y axis is time; we converted these
526 to bins/cycle (on an inverted scale) and bins, respectively.

527 **Declarations**

528 **Ethics approval and consent to participate:** Not applicable

529 **Consent for publication:** Not applicable

530 **Availability of data and material**

531 The sequences and SNPs reported in this paper have been deposited with the National Center for
532 Biotechnology Information Sequence Read Archive <https://trace.ncbi.nlm.nih.gov/Traces/sra/>
533 (accession no. in progress) and in the IUScholarWorks Repository (hdl.handle.net/2022/20340).
534 Bacterial strains are available upon request

535 **Competing interests**

536 The authors declare no competing interests

537 **Funding**

538 This research was supported by US Army Research Office Multidisciplinary University Research
539 Initiative (MURI) Award W911NF-09-1-0444 to P.L.F. and H.T., the National Institutes of Health T32

540 GM007757 to B.A.N., and the US Army Undergraduate Research Apprenticeship Program to J. H. and S.
541 R

542 **Authors' contributions**

543 B.A.N. and P.L.F. designed the research, analyzed the data, and wrote the paper. B.A.N executed the
544 experiments. W.M., H.L., and H.T. performed the bioinformatic analyses. P.L.F. and H.T. supplied
545 resources. All authors read and approved the final manuscript.

546 **Acknowledgements**

547 We thank H. Bedwell-Ivers, C. Coplen, M. Durham, J. Eagan, N. Gruenhagen, J. A. Healy, N. Ivers,
548 C. Klineman., H. Lee, E. Popodi, I. Rameses, S. Riffert, H. Rivera, D. Simon, K. Smith, J. Townes, L. Tran,
549 and L. Whitson for technical help. Bacterial strains were kindly provided by R. Schaaper, R. Reyes-
550 Lamothe, D. Kearns, M. Konkol, and The National BioResource Project at the (Japanese) National
551 Institute of Genetics. We also thank S. E.Bell and X. Wang for technical help and discussions.

552 **References**

- 553 1. Foster PL, Hanson AJ, Lee H, Popodi EM, Tang H. On the mutational topology of the bacterial
554 genome. *G3* (Bethesda). 2013;3(3):399-407.
- 555 2. Dillon MM, Sung W, Lynch M, Cooper VS. Periodic variation of mutation rates in bacterial
556 genomes associated with replication timing. *MBio*. 2018;9(4).
- 557 3. Dillon MM, Sung W, Sebra R, Lynch M, Cooper VS. Genome-wide biases in the rate and molecular
558 spectrum of spontaneous mutations in *Vibrio cholerae* and *Vibrio fischeri*. *Mol Biol Evol*. 2017;34(1):93-
559 109.

- 560 4. Wei W, Xiong L, Ye YN, Du MZ, Gao YZ, Zhang KY, et al. Mutation landscape of base substitutions,
561 duplications, and deletions in the representative current cholera pandemic strain. *Genome Biol Evol.*
562 2018;10(8):2072-85.
- 563 5. Long H, Sung W, Miller SF, Ackerman MS, Doak TG, Lynch M. Mutation rate, spectrum, topology,
564 and context-dependency in the DNA mismatch repair-deficient *Pseudomonas fluorescens* ATCC948.
565 *Genome Biol Evol.* 2014;7(1):262-71.
- 566 6. Dettman JR, Sztepanacz JL, Kassen R. The properties of spontaneous mutations in the
567 opportunistic pathogen *Pseudomonas aeruginosa*. *BMC Genomics.* 2016;17:27.
- 568 7. Lee H, Popodi E, Tang H, Foster PL. Rate and molecular spectrum of spontaneous mutations in
569 the bacterium *Escherichia coli* as determined by whole-genome sequencing. *Proceedings of the*
570 *National Academy of Sciences of the United States of America.* 2012;109(41):E2774-E83.
- 571 8. Marinus MG. DNA Mismatch Repair. *EcoSal Plus.* 2012; doi:10.1128/ecosalplus.7.2.5
- 572 9. Ganai RA, Johansson E. DNA replication—a matter of fidelity. *Mol Cell.* 2016;62(5):745-55.
- 573 10. Niccum BA, Lee H, MohammedIsmail W, Tang H, Foster PL. The spectrum of replication errors in
574 the absence of error correction assayed across the whole genome of *Escherichia coli*. *Genetics.*
575 2018;209(4):1043-54.
- 576 11. Foster PL, Niccum BA, Popodi E, Townes JP, Lee H, MohammedIsmail W, et al. Determinants of
577 base-pair substitution patterns revealed by whole-genome sequencing of DNA mismatch repair
578 defective *Escherichia coli*. *Genetics.* 2018;209(4):1029-42.
- 579 12. Valens M, Penaud S, Rossignol M, Cornet F, Boccard F. Macrodomain organization of the
580 *Escherichia coli* chromosome. *EMBO J.* 2004;23(21):4330-41.

- 581 13. Jinks-Robertson S, Bhagwat AS. Transcription-associated mutagenesis. *Annu Rev Genet.*
582 2014;48:341-59.
- 583 14. Rasouly A, Pani B, Nudler E. A magic spot in genome maintenance. *Trends Genet.* 2017;33(1):58-
584 67.
- 585 15. Zhang X, Zhang X, Zhang X, Liao Y, Song L, Zhang Q, et al. Spatial vulnerabilities of the *Escherichia*
586 *coli* genome to spontaneous mutations revealed with improved duplex sequencing. *Genetics.*
587 2018;210(2):547-58.
- 588 16. Withey JH, Friedman DI. A salvage pathway for protein structures: tmRNA and trans-translation.
589 *Annu Rev Microbiol.* 2003;57:101-23.
- 590 17. Kogoma T. Stable DNA replication: interplay between DNA replication, homologous
591 recombination, and transcription. *Microbiol and Molec Biol Rev.* 1997;61:212-38.
- 592 18. Maduike NZ, Tehranchi AK, Wang JD, Kreuzer KN. Replication of the *Escherichia coli* chromosome
593 in RNase HI-deficient cells: multiple initiation regions and fork dynamics. *Mol Microbiol.* 2014;91(1):39-
594 56.
- 595 19. Wang X, Lesterlin C, Reyes-Lamothe R, Ball G, Sherratt DJ. Replication and segregation of an
596 *Escherichia coli* chromosome with two replication origins. *Proceedings of the National Academy of*
597 *Sciences of the United States of America.* 2011;108(26):E243-50.
- 598 20. Ivanova D, Taylor T, Smith SL, Dimude JU, Upton AL, Mehrjouy MM, et al. Shaping the landscape
599 of the *Escherichia coli* chromosome: replication-transcription encounters in cells with an ectopic
600 replication origin. *Nucleic Acids Res.* 2015;43(16):7865-77.
- 601 21. Waldminghaus T, Skarstad K. The *Escherichia coli* SeqA protein. *Plasmid.* 2009;61(3):141-50.

- 602 22. Sutura VA, Jr., Lovett ST. The role of replication initiation control in promoting survival of
603 replication fork damage. *MolMicrobiol.* 2006;60(1):229-39.
- 604 23. Sanchez-Romero MA, Busby SJ, Dyer NP, Ott S, Millard AD, Grainger DC. Dynamic distribution of
605 SeqA protein across the chromosome of *Escherichia coli* K-12. *MBio.* 2010;1(1):e00012-10.
- 606 24. Weitao T, Nordstrom K, Dasgupta S. *Escherichia coli* cell cycle control genes affect chromosome
607 superhelicity. *EMBO Rep.* 2000;1(6):494-9.
- 608 25. Lobner-Olesen A, Marinus MG, Hansen FG. Role of SeqA and Dam in *Escherichia coli* gene
609 expression: a global/microarray analysis. *Proceedings of the National Academy of Sciences of the*
610 *United States of America.* 2003;100(8):4672-7.
- 611 26. Waldminghaus T, Skarstad K. ChIP on Chip: surprising results are often artifacts. *BMC Genomics.*
612 2010;11:414.
- 613 27. Sun L, Fuchs JA. *Escherichia coli* ribonucleotide reductase expression is cell cycle regulated. *Mol*
614 *Biol Cell.* 1992;3(10):1095-105.
- 615 28. Gon S, Camara JE, Klungsoyr HK, Crooke E, Skarstad K, Beckwith J. A novel regulatory mechanism
616 couples deoxyribonucleotide synthesis and DNA replication in *Escherichia coli*. *EMBO J.*
617 2006;25(5):1137-47.
- 618 29. Cooper S, Helmstetter CE. Chromosome replication and the division cycle of *Escherichia coli* B/r. *J*
619 *Mol Biol.* 1968;31(3):519-40.
- 620 30. Claret L, Rouviere-Yaniv J. Variation in HU composition during growth of *Escherichia coli*: the
621 heterodimer is required for long term survival. *J Mol Biol.* 1997;273(1):93-104.
- 622 31. Dorman CJ. Function of nucleoid-associated proteins in chromosome structuring and
623 transcriptional regulation. *J Mol Microbiol Biotechnol.* 2014;24(5-6):316-31.

- 624 32. Kahramanoglou C, Seshasayee AS, Prieto AI, Ibberson D, Schmidt S, Zimmermann J, et al. Direct
625 and indirect effects of H-NS and Fis on global gene expression control in *Escherichia coli*. *Nucleic Acids*
626 *Res.* 2011;39(6):2073-91.
- 627 33. Torrents E, Grinberg I, Gorovitz-Harris B, Lundstrom H, Borovok I, Aharonowitz Y, et al. NrdR
628 controls differential expression of the *Escherichia coli* ribonucleotide reductase genes. *J Bacteriol.*
629 2007;189(14):5012-21.
- 630 34. Lane HE, Denhardt DT. The rep mutation. IV. Slower movement of replication forks in *Escherichia*
631 *coli* rep strains. *J Mol Biol.* 1975;97(1):99-112.
- 632 35. Guy CP, Atkinson J, Gupta MK, Mahdi AA, Gwynn EJ, Rudolph CJ, et al. Rep provides a second
633 motor at the replisome to promote duplication of protein-bound DNA. *Mol Cell.* 2009;36(4):654-66.
- 634 36. Boubakri H, de Septenville AL, Viguera E, Michel B. The helicases DinG, Rep and UvrD cooperate
635 to promote replication across transcription units in vivo. *EMBO J.* 2010;29(1):145-57.
- 636 37. Myka KK, Hawkins M, Syeda AH, Gupta MK, Meharg C, Dillingham MS, et al. Inhibiting translation
637 elongation can aid genome duplication in *Escherichia coli*. *Nucleic Acids Res.* 2017;45(5):2571-84.
- 638 38. Heller RC, Marians KJ. Non-replicative helicases at the replication fork. *DNA Repair (Amst).*
639 2007;6(7):945-52.
- 640 39. Sandler SJ, Marians KJ. Role of PriA in replication fork reactivation in *Escherichia coli*. *J Bact.*
641 2000;182:9-13.
- 642 40. Duggin IG, Wake RG, Bell SD, Hill TM. The replication fork trap and termination of chromosome
643 replication. *MolMicrobiol.* 2008;70(6):1323-33.

- 644 41. Mercier R, Petit MA, Schbath S, Robin S, El Karoui M, Boccard F, et al. The MatP/matS site-specific
645 system organizes the terminus region of the *E. coli* chromosome into a macrodomain. *Cell*.
646 2008;135(3):475-85.
- 647 42. Espeli O, Borne R, Dupaigne P, Thiel A, Gigant E, Mercier R, et al. A MatP-divisome interaction
648 coordinates chromosome segregation with cell division in *E. coli*. *EMBO J*. 2012;31(14):3198-211.
- 649 43. Syeda AH, Hawkins M, McGlynn P. Recombination and replication. *Cold Spring Harb Perspect*
650 *Biol*. 2014;6(11):a016550.
- 651 44. Louarn JM, Louarn J, Francois V, Patte J. Analysis and possible role of hyperrecombination in the
652 termination region of the *Escherichia coli* chromosome. *J Bacteriol*. 1991;173(16):5097-104.
- 653 45. Bierne H, Ehrlich SD, Michel B. The replication termination signal *terB* of the *Escherichia coli*
654 chromosome is a deletion hot spot. *EMBO J*. 1991;10(9):2699-705.
- 655 46. Louarn J, Cornet F, Francois V, Patte J, Louarn JM. Hyperrecombination in the terminus region of
656 the *Escherichia coli* chromosome: possible relation to nucleoid organization. *J Bacteriol*.
657 1994;176(24):7524-31.
- 658 47. Corre J, Cornet F, Patte J, Louarn JM. Unraveling a region-specific hyper-recombination
659 phenomenon: genetic control and modalities of terminal recombination in *Escherichia coli*. *Genetics*.
660 1997;147(3):979-89.
- 661 48. Cox MM. Regulation of bacterial RecA protein function. *Crit Rev Biochem Mol Biol*.
662 2007;42(1):41-63.
- 663 49. Little JW, Harper JE. Identification of the *lexA* gene product of *Escherichia coli* K-12. *Proceedings*
664 *of the National Academy of Sciences of the United States of America*. 1979;76(12):6147-51.

- 665 50. Prieto AI, Kahramanoglou C, Ali RM, Fraser GM, Seshasayee AS, Luscombe NM. Genomic analysis
666 of DNA binding and gene regulation by homologous nucleoid-associated proteins IHF and HU in
667 *Escherichia coli* K12. *Nucleic Acids Res.* 2012;40(8):3524-37.
- 668 51. Sobetzko P, Travers A, Muskhelishvili G. Gene order and chromosome dynamics coordinate
669 spatiotemporal gene expression during the bacterial growth cycle. *ProcNatlAcadSciUSA.*
670 2012;109(2):E42-E50.
- 671 52. Cho BK, Knight EM, Barrett CL, Palsson BO. Genome-wide analysis of Fis binding in *Escherichia*
672 *coli* indicates a causative role for A-/AT-tracts. *Genome Res.* 2008;18(6):900-10.
- 673 53. Wang W, Li GW, Chen C, Xie XS, Zhuang X. Chromosome organization by a nucleoid-associated
674 protein in live bacteria. *Science.* 2011;333(6048):1445-9.
- 675 54. Lang B, Blot N, Bouffartigues E, Buckle M, Geertz M, Gualerzi CO, et al. High-affinity DNA binding
676 sites for H-NS provide a molecular basis for selective silencing within proteobacterial genomes. *Nucleic*
677 *Acids Res.* 2007;35(18):6330-7.
- 678 55. Bouffartigues E, Buckle M, Badaut C, Travers A, Rimsky S. H-NS cooperative binding to high-
679 affinity sites in a regulatory element results in transcriptional silencing. *Nat Struct Mol Biol.*
680 2007;14(5):441-8.
- 681 56. Wolf SG, Frenkiel D, Arad T, Finkel SE, Kolter R, Minsky A. DNA protection by stress-induced
682 biocrystallization. *Nature.* 1999;400(6739):83-5.
- 683 57. Foster PL, Lee H, Popodi E, Townes JP, Tang H. Determinants of spontaneous mutation in the
684 bacterium *Escherichia coli* as revealed by whole-genome sequencing. *Proceedings of the National*
685 *Academy of Sciences of the United States of America.* 2015;112(44):E5990-E599.

- 686 58. Duigou S, Boccard F. Long range chromosome organization in *Escherichia coli*: The position of the
687 replication origin defines the non-structured regions and the Right and Left macrodomains. PLoS
688 Genet. 2017;13(5):e1006758.
- 689 59. Dupaigne P, Tonthat NK, Espeli O, Whitfill T, Boccard F, Schumacher MA. Molecular basis for a
690 protein-mediated DNA-bridging mechanism that functions in condensation of the *E. coli* chromosome.
691 Mol Cell. 2012;48(4):560-71.
- 692 60. Liroy VS, Cournac A, Marbouty M, Duigou S, Mozziconacci J, Espeli O, et al. Multiscale structuring
693 of the *E. coli* chromosome by nucleoid-associated and condensin proteins. Cell. 2018;172(4):771-83
694 e18.
- 695 61. Thiel A, Valens M, Vallet-Gely I, Espeli O, Boccard F. Long-range chromosome organization in *E.*
696 *coli*: a site-specific system isolates the Ter macrodomain. PLoS Genet. 2012;8(4):e1002672.
- 697 62. Salgado H, Peralta-Gil M, Gama-Castro S, Santos-Zavaleta A, Muniz-Rascado L, Garcia-Sotelo JS, et
698 al. RegulonDB v8.0: omics data sets, evolutionary conservation, regulatory phrases, cross-validated
699 gold standards and more. Nucleic Acids Res. 2013;41(Database issue):D203-13.
- 700 63. Guo F, Adhya S. Spiral structure of *Escherichia coli* HU α provides foundation for DNA
701 supercoiling. Proceedings of the National Academy of Sciences of the United States of America.
702 2007;104(11):4309-14.
- 703 64. van Noort J, Verbrugge S, Goosen N, Dekker C, Dame RT. Dual architectural roles of HU:
704 formation of flexible hinges and rigid filaments. Proceedings of the National Academy of Sciences of
705 the United States of America. 2004;101(18):6969-74.

- 706 65. Pinson V, Takahashi M, Rouviere-Yaniv J. Differential binding of the *Escherichia coli* HU,
707 homodimeric forms and heterodimeric form to linear, gapped and cruciform DNA. J Mol Biol.
708 1999;287(3):485-97.
- 709 66. Bonnefoy E, Almeida A, Rouviere-Yaniv J. Lon-dependent regulation of the DNA binding protein
710 HU in *Escherichia coli*. Proceedings of the National Academy of Sciences of the United States of
711 America. 1989;86(20):7691-5.
- 712 67. Berger M, Farcas A, Geertz M, Zhelyazkova P, Brix K, Travers A, et al. Coordination of genomic
713 structure and transcription by the main bacterial nucleoid-associated protein HU. EMBO Rep.
714 2010;11(1):59-64.
- 715 68. Browning DF, Grainger DC, Busby SJ. Effects of nucleoid-associated proteins on bacterial
716 chromosome structure and gene expression. Curr Opin Microbiol. 2010;13(6):773-80.
- 717 69. Grainger DC, Hurd D, Goldberg MD, Busby SJ. Association of nucleoid proteins with coding and
718 non-coding segments of the *Escherichia coli* genome. Nucleic Acids Res. 2006;34(16):4642-52.
- 719 70. Blot N, Mavathur R, Geertz M, Travers A, Muskhelishvili G. Homeostatic regulation of
720 supercoiling sensitivity coordinates transcription of the bacterial genome. EMBO Rep. 2006;7(7):710-5.
- 721 71. Benjamini Y, Hochberg Y. Controlling the false discovery rate - a practical and powerful approach
722 to multiple testing. J Roy Stat Soc Ser B (Stat Method). 1995;57(1):289-300.
- 723 72. Grinsted A, Moore JC, Jevrejeva S. Application of the cross wavelet transform and wavelet
724 coherence to geophysical time series. Nonlinear Processes in Geophysics. 2004;11:561-6.
- 725 73. Maraun D, Kurths J. Cross wavelet analysis: significance testing and pitfalls. Nonlinear Processes
726 in Geophysics. 2004;11:505-14.

727

Table 1. Pearson's correlation, ρ , of each strain versus MMR⁻

		Whole									
		Chromosome		Right Replichore		Left Replichore		Origin		Terminus	
		Bins 1 to 46		Bins 1 to 23		Bins 46 to 24		Bins 1 to 13, 46 to 34		Bins 14 to 33	
Strain	Description	ρ	P ^a	ρ	P ^a	ρ	P ^a	ρ	P ^a	ρ	P ^a
Collective ^b	MMR ⁻	—	—	—	—	—	—	—	—	—	—
Collective	MMR ⁻ minus A:T ts at NAC/NTG	0.94	<0.001	0.93	<0.001	0.96	<0.001	0.97	<0.001	0.71	0.004
PFM421	Δ <i>rnhA</i> Δ <i>mutL</i>	0.74	<0.001	0.63	0.002	0.84	<0.001	0.81	<0.001	0.47	0.075
PFM669	Δ <i>mutL</i> (AB1157)	0.59	<0.001	0.40	0.064	0.75	<0.001	0.71	<0.001	0.45	0.079
PFM430/ 431	<i>oriC</i> ⁺ <i>oriZ</i> ⁺ Δ <i>mutL</i> (AB1157)	0.75	<0.001	0.71	<0.001	0.81	<0.001	0.83	<0.001	0.46	0.075
PFM426	Δ <i>oriC</i> <i>oriZ</i> ⁺ Δ <i>mutL</i> (AB1157)	0.39	0.008	0.21	0.34	0.62	0.003	0.40	0.044	0.41	0.11
PFM533/ 534	Δ <i>seqA</i> Δ <i>mutL</i>	0.49	0.001	0.71	<0.001	0.27	0.23	0.53	0.006	0.38	0.14
PFM5 ^b	Δ <i>mutL</i> on minimal medium	0.50	0.001	0.40	0.069	0.61	0.003	0.57	0.003	0.58	0.029

PFM343 ^b	<i>ΔmutS</i> on minimal										
	medium	0.18	0.22	0.18	0.41	0.18	0.41	0.21	0.31	0.22	0.38
PFM343 ^b	<i>ΔmutS</i> on diluted LB	0.84	<0.001	0.84	<0.001	0.85	<0.001	0.87	<0.001	0.71	0.004
PFM343 ^b	<i>ΔmutS</i> on supplemented										
	minimal medium	0.81	<0.001	0.82	<0.001	0.81	<0.001	0.83	<0.001	0.65	0.008
PFM342 ^b	<i>ΔmutS</i> at low										
	temperature	0.57	<0.001	0.60	0.003	0.53	0.013	0.69	<0.001	-0.02	0.95
PFM799	<i>ΔnrdR ΔmutL</i>	0.49	0.001	0.58	0.005	0.39	0.080	0.69	<0.001	-0.31	0.24
PFM677	<i>Δrep ΔmutL</i>	0.48	0.001	0.49	0.022	0.48	0.027	0.62	0.001	-0.12	0.67
PFM256	<i>Δtus ΔmutL</i>	0.82	<0.001	0.79	<0.001	0.85	<0.001	0.87	<0.001	0.70	0.004
PFM257	<i>ΔmatP ΔmutL</i>	0.40	0.007	0.60	0.004	0.21	0.34	0.70	<0.001	-0.47	0.075
PFM422	<i>ΔrecA ΔmutL</i>	0.71	<0.001	0.70	<0.001	0.73	<0.001	0.85	<0.001	0.06	0.84
PFM424	<i>ΔrecA ΔmutS</i>	0.80	<0.001	0.78	<0.001	0.83	<0.001	0.91	<0.001	0.44	0.082
PFM456	<i>ΔrecB ΔmutL</i>	0.82	<0.001	0.87	<0.001	0.79	<0.001	0.89	<0.001	0.39	0.12
PFM118	<i>ΔumuDC ΔdinB ΔmutL</i>	0.59	<0.001	0.62	0.003	0.55	0.010	0.61	0.001	0.69	0.004
PFM120	<i>lexA3 ΔsulA ΔmutL</i>	0.82	<0.001	0.82	<0.001	0.83	<0.001	0.83	<0.001	0.80	0.001
PFM259	<i>ΔhupB ΔmutL</i>	0.73	<0.001	0.70	<0.001	0.77	<0.001	0.81	<0.001	0.57	0.031
PFM258	<i>ΔhupA ΔmutL</i>	0.49	0.001	0.43	0.053	0.58	0.005	0.67	<0.001	-0.23	0.38
PFM317/ 318	<i>Δfis ΔmutL</i>	0.51	<0.001	0.61	0.003	0.42	0.060	0.67	<0.001	-0.30	0.25
PFM482	<i>Δfis ΔmutS</i>	0.49	0.001	0.31	0.15	0.62	0.003	0.65	<0.001	-0.28	0.27

PFM741	<i>Δhns ΔmutL</i>	0.81	<0.001	0.81	<0.001	0.81	<0.001	0.88	<0.001	0.46	0.075
PFM713	<i>Δdps ΔmutL</i>	0.80	<0.001	0.84	<0.001	0.78	<0.001	0.89	<0.001	0.47	0.075
PFM163 ^c	<i>mutD5</i>	0.76	<0.001	0.79	<0.001	0.74	<0.001	0.82	<0.001	0.78	0.001
PFM165/397/399 ^c	<i>mutD5 ΔmutL</i>	0.64	<0.001	0.76	<0.001	0.52	0.014	0.86	<0.001	-0.46	0.075
Collective ^b	Wild type	0.36	0.014	0.41	0.061	0.31	0.17	0.37	0.065	0.51	0.060
Collective ^d	<i>Bacillus subtilis</i>										
	<i>mutS::Tn10</i>	0.52	<0.001	0.63	0.003	0.40	0.068	0.74	<0.001	-0.52	0.055

^a P values were adjusted for multiple comparisons using the Benjamini-Hochberg method (71) with the false discovery rate set at 25%

^b Data are from (11)

^c Data are from (10)

^d Data are combined from four MA experiments with DK2140 (NCIB3610 *mutS::Tn10*), DK2141 (NCIB3610 *mutS::Tn10*), DK2142 (NCIB3610 *mutS::Tn10 ΔcomI*), and DK2143 (NCIB3610 *mutS::Tn10 ΔcomI*). There were no differences in mutation rates or spectra among these strain

Table 2. Pearson's correlation, ρ , of right versus left replichore for each strain

Strain	Description	Whole Chromosome		Origin		Terminus	
		Bins 1 to 23, 46 to 24		Bins 1 to 13, 46 to 34		Bins 14 to 23, 33 to 24	
		ρ	P ^a	ρ	P ^a	ρ	P ^a
Collective ^b	MMR ⁻	0.91	<0.001	0.95	<0.001	0.66	0.23
Collective	MMR ⁻ minus A:T ts at NAC/NTG	0.89	<0.001	0.94	<0.001	0.42	0.60
PFM421	$\Delta rnhA \Delta mutL$	0.49	0.026	0.58	0.051	0.24	0.82
PFM669	$\Delta mutL$ (AB1157)	0.52	0.018	0.64	0.026	0.29	0.77
PFM430/ 431	<i>oriC⁺ oriZ⁺ $\Delta mutL$</i> (AB1157)	0.60	0.005	0.80	0.003	0.19	0.84
PFM426	$\Delta oriC oriZ+ \Delta mutL$ (AB1157)	0.28	0.22	0.33	0.31	-0.06	0.91
PFM533/ 534	$\Delta seqA \Delta mutL$	0.41	0.062	0.53	0.079	0.32	0.71
PFM5 ^b	$\Delta mutL$ on minimal medium	0.27	0.22	0.19	0.53	0.05	0.91
PFM343 ^b	$\Delta mutS$ on minimal medium	-0.02	0.93	0.32	0.31	-0.53	0.39
PFM343 ^b	$\Delta mutS$ on diluted LB	0.87	<0.001	0.93	<0.001	0.66	0.23
PFM343 ^b	$\Delta mutS$ on supplemented minimal medium	0.74	<0.001	0.79	0.003	0.54	0.39
PFM342 ^b	$\Delta mutS$ at low temperature	0.84	<0.001	0.89	<0.001	0.73	0.19
PFM799	$\Delta nrdR \Delta mutL$	0.79	<0.001	0.78	0.003	0.84	0.07
PFM677	$\Delta rep \Delta mutL$	0.43	0.053	0.58	0.051	-0.16	0.84
PFM256	$\Delta tus \Delta mutL$	0.70	0.001	0.88	<0.001	0.26	0.81
PFM257	$\Delta matP \Delta mutL$	0.45	0.042	0.40	0.20	0.72	0.19

PFM422	<i>ΔrecA ΔmutL</i>	0.66	0.001	0.81	0.003	0.11	0.88
PFM424	<i>ΔrecA ΔmutS</i>	0.64	0.002	0.80	0.003	0.07	0.91
PFM456	<i>ΔrecB ΔmutL</i>	0.67	0.001	0.78	0.003	0.03	0.94
PFM118	<i>ΔumuDC ΔdinB ΔmutL</i>	0.39	0.075	0.68	0.018	-0.13	0.87
PFM120	<i>lexA3 ΔsulA ΔmutL</i>	0.51	0.019	0.57	0.055	0.42	0.60
PFM259	<i>ΔhupB ΔmutL</i>	0.64	0.002	0.78	0.003	0.35	0.65
PFM258	<i>ΔhupA ΔmutL</i>	0.54	0.014	0.69	0.015	0.15	0.84
PFM317/ 318	<i>Δfis ΔmutL</i>	0.61	0.004	0.67	0.019	0.58	0.34
PFM482	<i>Δfis ΔmutS</i>	0.34	0.13	0.49	0.108	0.19	0.84
PFM741	<i>Δhns ΔmutL</i>	0.81	<0.001	0.85	0.001	0.60	0.33
PFM713	<i>Δdps ΔmutL</i>	0.52	0.017	0.77	0.004	-0.20	0.84
PFM163 ^c	<i>mutD5</i>	0.75	<0.001	0.77	0.004	0.52	0.39
PFM165/397/399 ^c	<i>mutD5 ΔmutL</i>	0.78	<0.001	0.88	<0.001	0.39	0.62
Collective ^b	Wild type	0.17	0.46	0.24	0.45	0.17	0.84
Collective ^d	<i>Bacillus subtilis mutS::Tn10</i>	0.73	<0.001	0.87	0.000	0.37	0.65

^a P values were adjusted for multiple comparisons using the Benjamini-Hochberg method (71) with the false discovery rate set at 25%

^b Data are from (11)

^c Data are from (10)

^d Data are combined from four MA experiments with DK2140 (NCIB3610 *mutS::Tn10*), DK2141 (NCIB3610 *mutS::Tn10*), DK2142 (NCIB3610 *mutS::Tn10* Δ *comI*), and DK2143 (NCIB3610 *mutS::Tn10* Δ *comI*). There were no differences in mutation rates or spectra among these strain

1 **Figure Legends**

2 **Figure 1.** The BPS density pattern is not due to transcription but is affected by moving the origin
3 of replication. For each plot the data were collected into 100 Kb bins starting at the origin of
4 replication on the left and continuing clockwise around the chromosome back to the origin on
5 the right. **Figure 1A.** The BPS density pattern of MMR-defective strains. Bars represent the
6 mean mutation rate in each bin calculated from the BPSs collected from 10 experiments with
7 MMR-defective strains. Error bars are the 95% CLs of the means. The grey line represents the
8 Daubechies wavelet transform of the binned data. The chromosomal macrodomains (MCs) are
9 indicated at the top of the plot: green, Ori MC; blue, Right and Left MC; red, Ter MC. **Figure 1B.**
10 The Daubechies wavelet transform of the binned reads from RNA-Seq samples taken during lag,
11 log, and stationary growth phases of the $\Delta mutL$ mutant strain, PFM144. The data used for the
12 wavelet transforms were the means of three biological replicates. Arrows indicate the positions
13 of the rRNA operons, but the reads from the ribosomal genes in those operons were not
14 included in the plot. **Figure 1C, D, E, and F.** The BPS density patterns (bars) and Daubechies
15 wavelet transforms (pink line) of the indicated mutant strains compared to the Daubechies
16 wavelet transform of the combined MMR⁻ strains (grey line). See text for a description of the
17 strains. In each plot the left-hand scale has been adjusted to bring the wavelets close together
18 for comparison. The red arrow in 1E indicates the position of *oriZ*. Strains: 1C, PFM421; 1D,
19 PFM430/431; 1E, PFM426; 1F, PFM533/534.

20 **Figure 2.** Altering the progression of DNA replication affects the BPS density pattern. For each
21 plot the data were collected into 100 Kb bins starting at the origin of replication on the left and
22 continuing clockwise around the chromosome back to the origin on the right. The BPS density

23 patterns (bars) and Daubechies wavelet transforms (pink lines) of the indicated strains are
24 compared to the Daubechies wavelet transform of the combined MMR⁻ strains (grey line). In
25 each plot the left-hand scale has been adjusted to bring the wavelets close together for
26 comparison. **Figure 2A, B, C, and D.** Altering the cellular growth rate by growing a $\Delta mutS$
27 mutant strain on different medium and at different temperatures differentially affects the BPS
28 density pattern. In the experiments shown in Plot A, C, and D, the cells grew at about half the
29 normal rate, whereas in the experiment shown in plot B they grew at the normal rate. Strains:
30 2A, 2B, and 2C, PFM343; 2D, PFM342. **Figure 2E and F.** Dysregulation of dNTP levels and loss of
31 Rep, the auxiliary replication helicase, affect the BPS density pattern. 2E, PFM799; 2F, PFM677.
32 **Figure 2G and H.** Loss of the Tus antihelicase has no effect, but loss of the terminus organizing
33 protein, MatP, changes the BPS density pattern across the chromosome. The arrows in Figure
34 2G mark the major Ter sites where Tus binds. The bar in Figure 2H shows the region in which
35 MatP binds. Strains: 2G, PFM256; 2H, PFM257.

36 **Figure 3.** Loss of RecA, HU α , or Fis changes the BPS pattern, but the SOS response and loss of
37 other NAPs do not. For a description of the plots, see the legend to Figure 2. **Figure 3A, B, and**
38 **C.** Loss of RecA alters the BPS density pattern in the terminus region, but not through its role as
39 a master regulator of the SOS response. RecA (Figure 3A) is *E. coli*'s major recombinase. The
40 *dinB* and *umuDC* genes (Figure 3B) encode the error-prone DNA polymerases, Pol IV and Pol V,
41 that are induced as part of the SOS response. The *lexA3* allele encodes a non-inducible
42 repressor of the SOS genes. Deletion of *sulA* prevents lethal filamentation after induction of the
43 SOS response (not relevant to this study). Strains: 3A, PFM422; 3B, PFM118; 3C, PFM120.

44 **Figure 3D, E, F, G, and H.** Loss of the HU α subunit of HU or of Fis changes the BPS density

45 pattern, but loss of the HU β subunit of HU, HNS, or DPS has only minor effects. Strains: 3D,
46 PFM259; 3E, PFM258; 3F, PFM317/318; 3G, PFM741/742; 3H, PFM713.

47 **Figure 4.** The BPS density pattern is a result of biased correction by replication proofreading
48 and MMR. For a description of the plots, see the legend to Figure 2. **Figure 4A and B.** A strain
49 with deficient proofreading but active MMR yields a BPS pattern similar to a MMR-defective
50 strain, but a strain with neither proofreading nor MMR does not. The *mutD5* allele encodes an
51 exonuclease deficient proofreader. Strains: 4A, PFM163; 4B, PFM165/397/399. **Figure 4C and**
52 **D.** The BPS density pattern in the wild-type strain does not match the pattern of either the
53 MMR-defective strain, or the *mutD5* mutant strain. The green line in Figure 1D is the
54 Daubechies wavelet transform of the *mutD5* mutant strain (pink line in Figure 4A). Strains: 4C
55 and D, eight strains with wild-type mutational phenotypes (see text). **Figure 4E.** MMR-defective
56 *B. subtilis* also has a symmetrical BPS density pattern, but it is different than *E. coli*'s pattern.
57 Strains: three *B. subtilis* mutant strains with the same mutational phenotype (see
58 supplementary Tables S1 and S3).

Figure 1

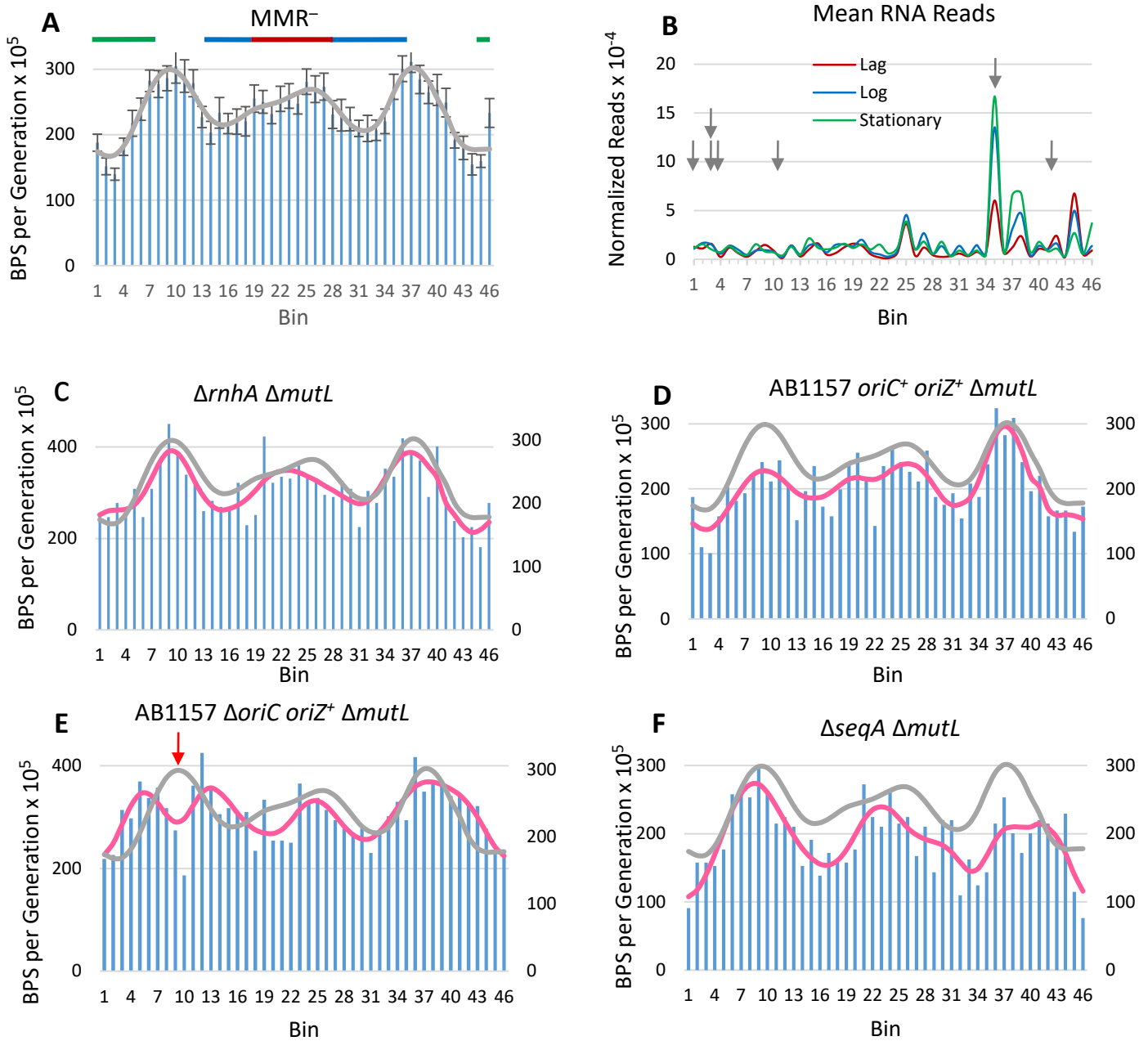


Figure 2

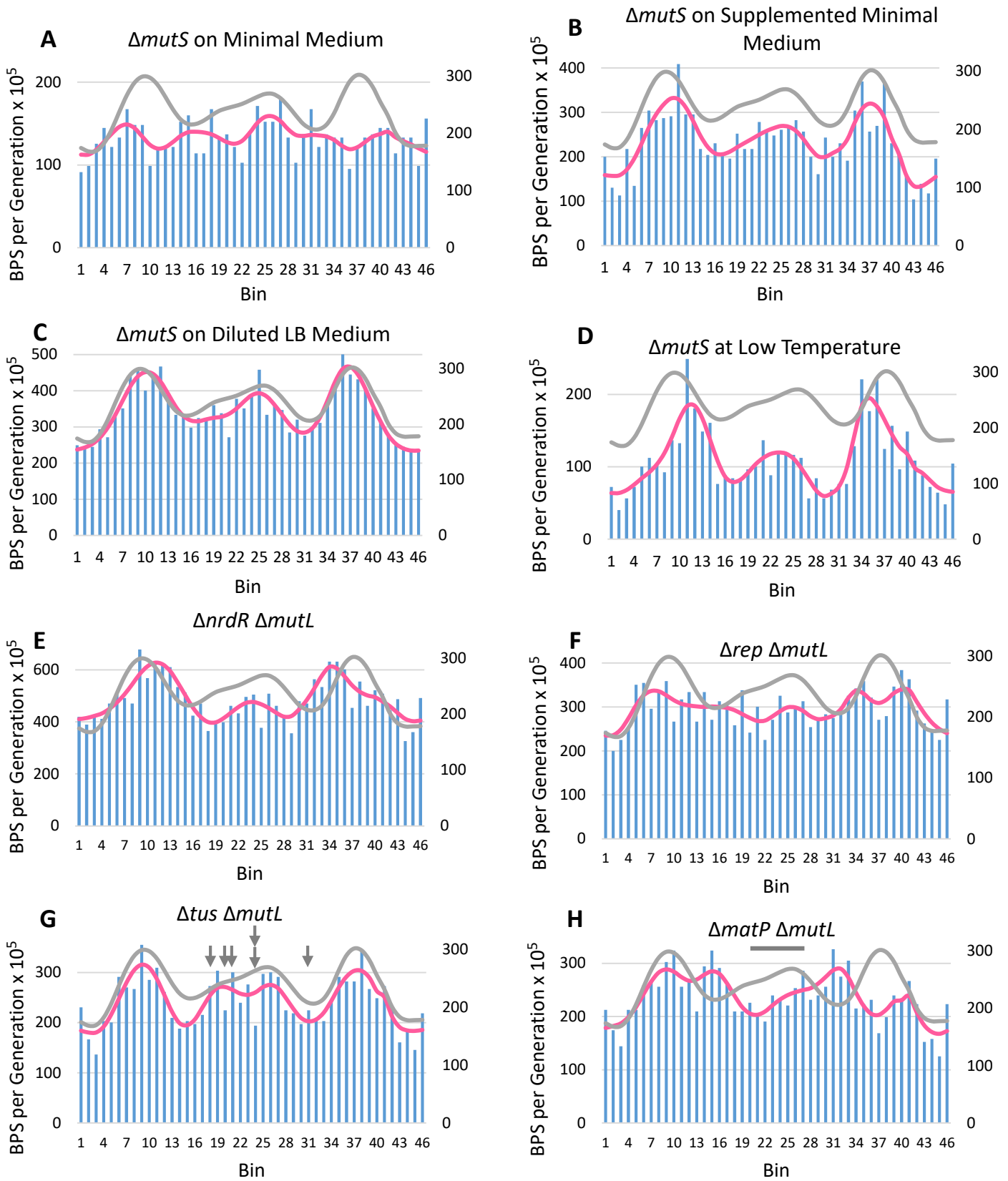


Figure 3

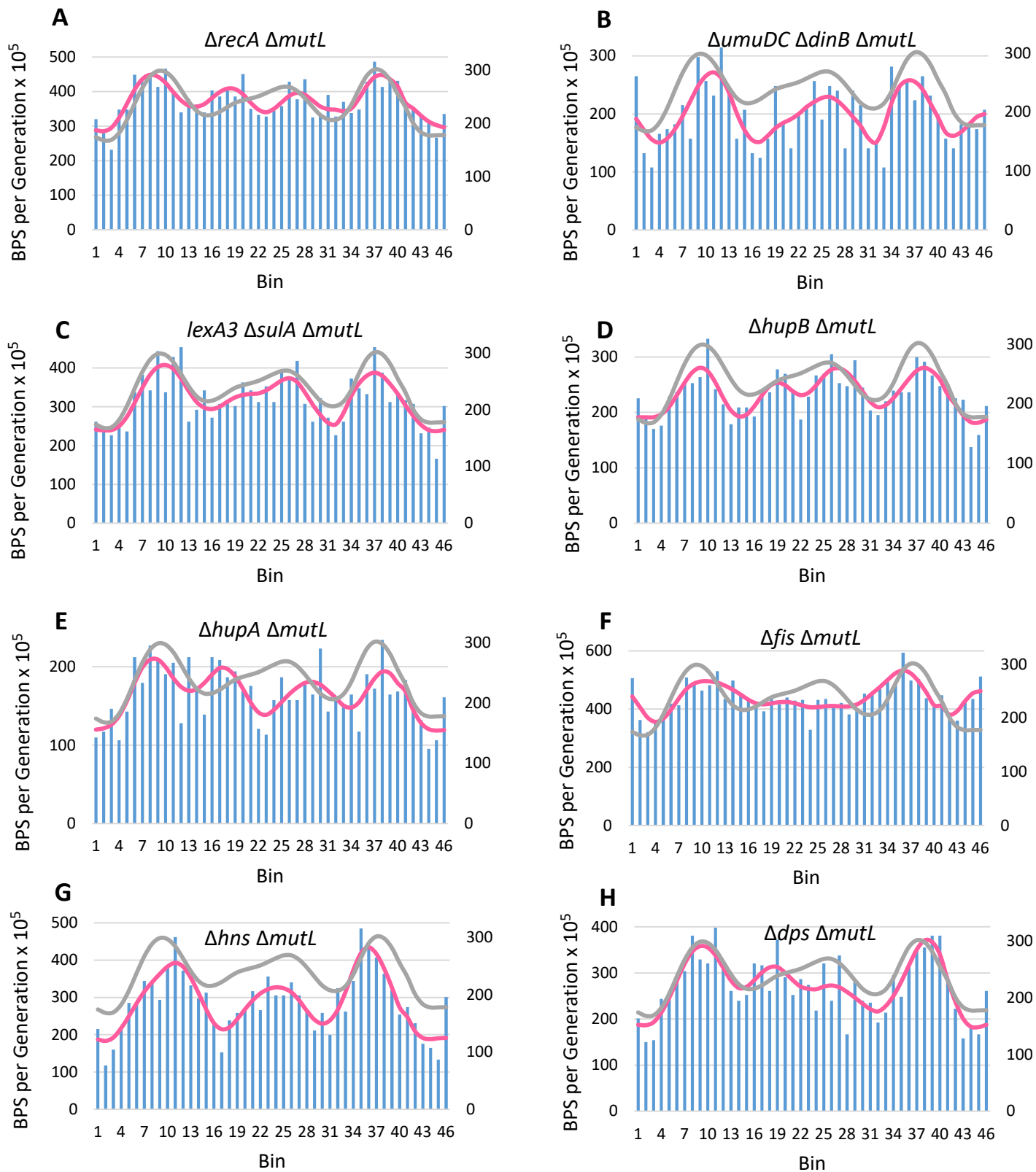
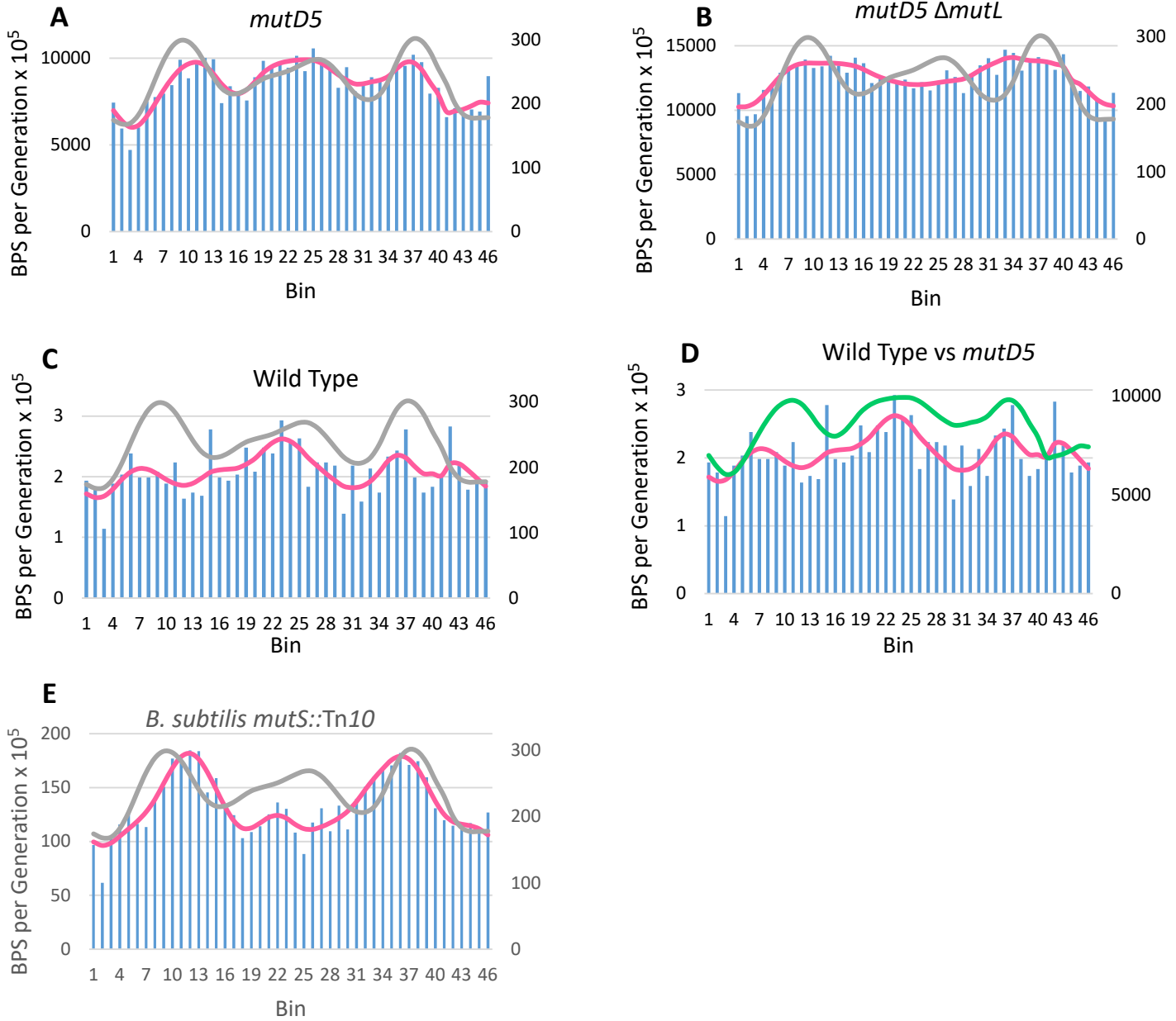


Figure 4



1 **Supplemental Material and Methods**

2 **Bacterial strains and media**

3 The strains used in this study are listed in Supplemental Table S1. All *E. coli* strains were derived from
4 PFM2 (1) or AB1157 (2). The *oriC⁺ oriZ⁺* and Δ *oriC oriZ⁺* strains were a gift from Rodrigo Reyes-
5 Lamothe (McGill University). The *mutD5* allele was obtained from Roel Schaaper (NIEHS). The deletion
6 mutations originated in the Keio collection (3) and were moved by P1 phage transduction (4); the Kn^r
7 element was removed by using FLP recombination (5). The deletions were confirmed by PCR analysis
8 using the oligonucleotides listed in Supplemental Table S2. The *B. subtilis* strains were derived from the
9 undomesticated ancestral strain NCIB3610 and were a gift from M.A. Konkol and D.B. Kearns (Indiana
10 University).

11 Rich medium was Miller Luria Broth (LB) (Difco; BD); minimal medium was Vogel-Bonner minimal
12 medium (VB min) with 0.2% glucose (6). When required, antibiotic concentrations were: carbenicillin
13 (Carb), 100 $\mu\text{g}/\text{ml}$; kanamycin (Kn), 50 $\mu\text{g}/\text{ml}$; nalidixic acid (Nal), 40 $\mu\text{g}/\text{ml}$; chloramphenicol (Cam), 30
14 $\mu\text{g}/\text{ml}$; and, rifampicin (Rif), 100 $\mu\text{g}/\text{ml}$. Half of these concentrations were used in minimal medium.

15 **Estimation of mutation rates from fluctuation assays**

16 Mutation rates were determined as described (7), using mutation to Nal^R or Rif^R . The Ma-Sandri-Sarkar
17 maximum likelihood method was used to calculate the mutation rates by using the FALCOR web tool
18 found at www.mitochondria.org/protocols/FALCOR.html (8).

19 **Mutation accumulation experiments**

20 The MA procedure has been described (1, 9, 10). The MA lines originated from single colonies isolated
21 from a founder colony, obtained by streaking from a freezer stock onto agar plates of the medium to
22 be used in the MA experiment. After incubation overnight at the experimental temperature, one well

23 isolated colony was excised from the agar plate, soaked for 30 minutes in 0.85% NaCl + 0.01% gelatin,
24 and then vortexed for 60 seconds. Appropriate dilutions for obtaining well-isolated colonies were then
25 plated onto the appropriate agar plates at the appropriate temperature to start MA lines. Plates were
26 incubated at 37°C for most experiments, or at 28°C for the experiment at low temperature. Each MA
27 line was periodically streaked for a single colony: on LB and supplemented VB min agar plates at 37°C,
28 this was done daily; on VB min and diluted LB agar plates at 37°C, and on LB plates at 28°C, this was
29 done every 48 hours. The number of passes required was determined by the preliminary mutation rate
30 obtained from a fluctuation assay. The parameters of the MA experiment including the number of lines
31 used for each strain and the total number of generations per experiment are given in Supplemental
32 Table S3.

33 **Estimation of generations**

34 The method to estimate that number of generations undergone in each MA experiment is described (1,
35 9). The diameter of the single colonies streaked was recorded daily, and then the number of cells in
36 colonies of different diameters was determined for each experiment as described (1). The daily colony
37 diameters were converted to generations and the results summed.

38 **Genomic DNA preparation, library construction, and sequencing**

39 Genomic DNA was isolated using PureLink Genomic DNA purification kit (Invitrogen) from a
40 predetermined amount of overnight LB culture inoculated from the freezer stocks made after the last
41 passage of the MA line. DNA concentration was measured on an Epoch Microplate Spectrophotometer
42 (BioTek Instruments, Inc.). The identity of the lines was confirmed before library construction by
43 verifying the presence of the expected gene deletions in the gDNA with diagnostic PCR using the
44 oligonucleotides in Supplemental Table S2. Libraries were made by the Indiana University Center for

45 Genomics and Bioinformatics and were sequenced using the Illumina HiSeq 2500 platform at the
46 University of New Hampshire Hubbart Center for Genome Studies or the Illumina NextSeq platform at
47 the Indiana University Center for Genomics and Bioinformatics.

48 **Sequence analysis**

49 SNP calling is described (1). The reference genome used for *E. coli* was NCBI reference sequence
50 NC_000913.2, and for *B. subtilis* was GenBank: CP020102.1. The Illumina reads were aligned to the
51 referenced genomes using the Burrows-Wheeler short-read alignment tool, BWA version 0.7.9 (11).

52 Poor sequence coverage resulted in some MA lines being eliminated. Cross-contamination can
53 occur during streaking, resulting in lines with identical mutations. If two lines shared over 50% of their
54 mutations then one of the lines was dropped from further analysis. If lines shared less than 50%, then
55 each shared mutation was assigned to one of the lines and dropped from the others. If lineage could
56 be established the shared mutation was assigned accordingly, otherwise the mutation was assigned
57 randomly.

58 **RNA sequencing**

59 The *E. coli* strain PFM144, which is PFM2 $\Delta mutL$ (10), was grown in LB and aliquots collected during lag
60 (OD = 0.022), log (OD = 0.3), and stationary (OD = 1.5) phase.. The number of cells collected was kept
61 constant for each growth phase. Cells were pelleted at 10,000gs for 10 min, 1ml of medium was added
62 and the cells were pelleted again at 10,000gs for 2 min. The pellets were then flash frozen in liquid
63 nitrogen and stored at -80°. Three biological triplicates were prepared for each growth phase.

64 RNA was extracted using FastRNA Pro Blue kit (MP Biomedicals). DNA was removed by using
65 TurboDNase (Ambion). DNA removal was confirmed with diagnostic PCR using primer pair “fis forward”
66 and “fis reverse” (Supplemental Table S2). rRNA was removed using RiboMinus magnetic beads kit

67 (Invitrogen). RNA concentration and purity was assessed with an Epoch Microplate Spectrophotometer
68 (BioTek Instruments, Inc.). Libraries were made by the Indiana University CGB and were sequenced at
69 UT Health Science Center on Illumina HiSeq 2500 platform.

Table S1. Bacterial strains used in this study

Strain	Relevant genotype	Donor	Recipient	Target gene	Reference
PFM2	MG1655 <i>rph</i> ⁺				(1)
PFM5	Δ <i>mutL</i>				(1)
WX320	Δ <i>oriC oriZ</i> ⁺ (AB1157)				(12)
WX340	<i>oriC</i> ⁺ <i>oriZ</i> ⁺ (AB1157)				(12)
PF11	AB1157				Lab strain
PFM118	Δ <i>umuDC</i> Δ <i>dinB</i> Δ <i>mutL</i>				(10)
PFM120	<i>lexA3</i> Δ <i>sulA</i> Δ <i>mutL</i>				This Study
PFM163	<i>mutD5</i>				(13)
PFM165/397/399	<i>mutD5</i> Δ <i>mutL</i>				(13)
PFM244	Δ <i>mutL</i> , <i>scarless</i>				(10)
PFM256	Δ <i>tus</i> Δ <i>mutL</i>	JW1602	PFM244	Δ <i>tus</i> ::Kn ^R	This Study
PFM257	Δ <i>matP</i> Δ <i>mutL</i>	JW0939	PFM244	Δ <i>matP</i> ::Kn ^R	This Study
PFM258	Δ <i>hupA</i> Δ <i>mutL</i>	JW3964	PFM244	Δ <i>hupA</i> ::Kn ^R	This Study
PFM259	Δ <i>hupB</i> Δ <i>mutL</i>	JW0430	PFM244	Δ <i>hupB</i> ::Kn ^R	This Study
PFM317/ 318	Δ <i>fis</i> Δ <i>mutL</i>	JW3229	PFM244	Δ <i>fis</i> ::Kn ^R	This Study
PFM342/343	Δ <i>mutS</i> , <i>scarless</i>				(10)
PFM421	Δ <i>rnhA</i> Δ <i>mutL</i>	JW0204	PFM244	Δ <i>rnhA</i> ::Kn ^R	This Study
PFM422	Δ <i>recA</i> Δ <i>mutL</i>	JW2669	PFM244	Δ <i>recA</i> ::Kn ^R	This Study

PFM424	<i>ΔrecA ΔmutS</i>	JW2669	PFM342	<i>ΔrecA::Kn^R</i>	This Study
PFM426	<i>ΔoriC oriZ⁺ ΔmutL</i> (AB1157)	JW4128	WX320	<i>ΔmutL::Kn^R</i>	This Study
PFM430/ 431	<i>oriC⁺ oriZ⁺ ΔmutL</i> (AB1157)	JW4128	WX340	<i>ΔmutL::Kn^R</i>	This Study
PFM456	<i>ΔrecB ΔmutL</i>	JW2788	PFM244	<i>ΔrecB::Kn^R</i>	This Study
PFM482	<i>Δfis ΔmutS</i>	JW3229	PFM343	<i>Δfis::Kn^R</i>	This Study
PFM533/ 534	<i>ΔseqA ΔmutL</i>	JW0674	PFM244	<i>ΔseqA::Kn^R</i>	This Study
PFM661	<i>ΔhupA ΔrecA ΔmutL</i>	JW2669	PFM258	<i>ΔrecA::Kn^R</i>	This Study
PFM669	<i>ΔmutL</i> (AB1157)	JW4128	PF11	<i>ΔmutL::Kn^R</i>	This Study
PFM677	<i>Δrep ΔmutL</i>	JW5604	PFM244	<i>Δrep::Kn^R</i>	This Study
PFM713	<i>Δdps ΔmutL</i>	JW0797	PFM244	<i>Δdps::Kn^R</i>	This Study
PFM741	<i>Δhns ΔmutL</i>	JW1225-2	PFM244	<i>Δhns::Kn^R</i>	This Study
PFM799	<i>ΔnrdR ΔmutL</i>	JW0403	PFM244	<i>ΔnrdR::Kn^R</i>	This Study
DK2140/2141/ 2142/2143	<i>Bacillus subtilis mutS::Tn10</i>				M. Konkol & D. Kearns, personal communication

70 In all strains the Kn^R element was removed by FLP recombination (5).

71 Scarless: Scarless gene deletion using a cat-I-SceI cassette (14).

72

Table S2. Oligonucleotides used in this study

Relevant gene	Name	Sequence	Reference
<i>mutL</i>	mutL Fw	5'-GCCTGCGCAATTACTTCCTTG-3'	(1)
	mutL Rv	5'-CGCAGCTCAATGGCTAACGC-3'	
<i>mutS</i>	mutS FW	5'-CACGAGAGATACGCTTGCC-3'	This study
	mutS RV	5'-TCGTGGTTGCCTTAAACCGA-3'	
<i>oriC</i>	mioC_2958 FW	5'-CAAATAAGTATACAGATCGTG-3'	This study
	oriC dwnstrmRV	5'-CTTTGTCGGCTTGAGAAAGAC-3'	
<i>oriZ</i>	yahL1146FW	5'-GAGATGATGCGCGATTAAATG-3'	This study
	yahMupstrmRV	5'-CCCCGTACCATACAACAATC-3'	
<i>rnhA</i>	rnhA_dwnstrm RV	5'-CATCGGATTTAGCGTTAAAG-3'	This study
	rnhA_dwnstrm FW	5'-CTTTAACGCTAAATCCGATG-3'	
<i>seqA</i>	seqAFW	5'-CGAGTTTGTGCGTCCGATTC-3'	This study
	seqARV	5'-GATGGCATTGGAAACGGCAG-3'	
<i>tus</i>	tus FW	5'-CTCGTGCAAGGCCATTATGC-3'	This study
	tus RV	5'-AGTTTGACAGCTGGGTACGG-3'	
<i>matP</i>	matP FW	5'-ACAATACTCCTGGCATGGGC-3'	This study
	matP RV	5'-TGACGCTTACAACCAGGGTC-3'	
<i>recA</i>	recAF0102	5'-GCATTGCAGACCTTGTGGC-3'	This study
	recAR1134	5'-CGACGGGATGTTGATTCTG-3'	
<i>rnhA</i>	rnhA_dwnstrm RV	5'-CATCGGATTTAGCGTTAAAG-3'	This study
	rnhA_dwnstrm FW	5'-CTTTAACGCTAAATCCGATG-3'	

<i>recD</i>	recD_RV	5'-GACCACGCGCAGTATTCACT-3'	This study
	recD_FW	5'-GGGTGAAGACAGTTCGGCTT-3'	
<i>recB</i>	recB_RV	5'-GTTTCATCTCCCCTGCTGACC-3'	This study
	recB_FW	5'-CGTTTTTCCCAACCGCAGAG-3'	
<i>fis</i>	fisRV	5'-CTTTTTCAGAACGCGGTGGC-3'	This study
	fisFW	5'-GGAACACGCTCCAAATGACC-3'	
<i>hupA</i>	hupAFW	5'-CAGGCTGGTCGCGAAATGAG-3'	This study
	hupARV	5'-GCTAAACACGGCAAGCAGATG-3'	
<i>hupB</i>	hupBFW	5'-CTGTGAAGCGCATTGAGGAAG-3'	This study
	hupBRV	5'-CTTGAGCACGAGACTGTTTGC-3'	
<i>dps</i>	dpsFW_G	5'-GGGGTCTACGCTGACAGTAC-3'	This study
	dpsRV_BAN	5'-GATGCACCATTCTGGGGCACC-3'	
<i>hns</i>	hnsRV_G	5'-GTGGTAGAAAAACCGAAAGC-3'	This study
	hnsFW_G	5'-CATGAATCAGGAAGTTTTAAC-3'	
<i>rep</i>	repRv	5'-CTGTTGACCTTGACGCTTCC-3'	This study
	repFw	5'-CTTTGGCCCAACGAATCTGC-3'	

Table S3. Experimental data

Strain	Description	No. of BPSs	No. of MA lines	Total no. of generations	BPSs per generation x 10 ³	95% CL
*Collective	MMR ⁻	30061	334	264958	113	2
PFM421	<i>ΔrnhA ΔmutL</i>	3198	39	22690	141	7
PFM669	<i>ΔmutL</i> (AB1157)	1334	33	18850	71	6
PFM430/ 431	<i>oriC⁺ oriZ⁺ ΔmutL</i> (AB1157)	3150	65	33607	94	6
PFM426	<i>ΔoriC oriZ⁺ ΔmutL</i> (AB1157)	3544	45	25176	141	9
PFM533/ 534	<i>ΔseqA ΔmutL</i>	1855	44	20927	89	7
*PFM5m	<i>ΔmutL</i> on minimal medium	1435	48	28197	51	3
*PFM343m	<i>ΔmutS</i> on minimal medium	1608	46	26280	61	4
*PFM343VBs	<i>ΔmutS</i> on supplemented minimal medium	2476	39	23017	108	5
*PFM343dLB	<i>ΔmutS</i> on diluted LB	3546	40	22495	158	8
*PFM342LTM	<i>ΔmutS</i> at low temperature	1259	44	24875	51	5
PFM799	<i>ΔnrdR ΔmutL</i>	5272	42	23581	224	12
PFM677	<i>Δrep ΔmutL</i>	3258	43	23961	136	7
PFM256	<i>Δtus ΔmutL</i>	3672	28	32967	111	10
PFM257	<i>ΔmatP ΔmutL</i>	3979	33	36725	108	7

PFM422	<i>ΔrecA ΔmutL</i>	6797	40	39713	171	11
PFM424	<i>ΔrecA ΔmutS</i>	6266	36	36340	172	11
PFM456	<i>ΔrecB ΔmutL</i>	3321	46	20598	161	9
*PFM118	<i>ΔumuDC ΔdinB ΔmutL</i>	1110	23	12078	92	41
PFM120	<i>lexA3 ΔsuaA ΔmutL</i>	2909	33	19853	147	13
PFM259	<i>ΔhupB ΔmutL</i>	3910	32	36390	107	8
PFM258	<i>ΔhupA ΔmutL</i>	2075	26	27315	76	7
PFM317/ 318	<i>Δfis ΔmutL</i>	7616	35	37731	202	14
PFM482	<i>Δfis ΔmutS</i>	4669	40	22687	206	12
PFM741	<i>Δhns ΔmutL</i>	3367	46	25551	132	5
PFM713	<i>Δdps ΔmutL</i>	2927	40	23377	125	8
†PFM163	<i>mutD5</i>	13625	26	3481	3915	344
†PFM165/397/399	<i>mutD5 ΔmutL</i>	40686	75	7012	5802	456
*Collective	Wild Type	1933	341	2015066	0.96	0.10
‡Collective	<i>Bacillus subtilis mutS::Tn10</i>	10551	71	171805	61	3

*Data are from (10)

†Data are from (13)

‡Data are combined from four MA experiments with DK2140 (NCIB3610 *mutS::Tn10*), DK2141 (NCIB3610 *mutS::Tn10*), DK2142 (NCIB3610 *mutS::Tn10 ΔcomI*), and DK2143 (NCIB3610 *mutS::Tn10 ΔcomI*). There were no differences in mutation rates or spectra among these strains

74 **Supplemental References**

75

76 1. Lee H, Popodi E, Tang H, Foster PL. Rate and molecular spectrum of spontaneous
77 mutations in the bacterium *Escherichia coli* as determined by whole-genome sequencing.

78 Proceedings of the National Academy of Sciences of the United States of America.

79 2012;109(41):E2774-E83.

80 2. Dewitt SK, Adelberg EA. The Occurrence of a Genetic Transposition in a Strain of
81 *Escherichia Coli*. Genetics. 1962;47(5):577-85.

82 3. Baba T, Ara T, Hasegawa M, Takai Y, Okumura Y, Baba M, et al. Construction of
83 *Escherichia coli* K-12 in-frame, single-gene knockout mutants: the Keio collection. Mol Syst Biol.
84 2006;2:2006.

85 4. Miller JH. Experiments in molecular genetics. Cold Spring Harbor, N.Y.: Cold Spring Harbor
86 Laboratory; 1972 1972.

87 5. Datsenko KA, Wanner BL. One-step inactivation of chromosomal genes in *Escherichia coli*
88 K-12 using PCR products. Proc Natl Acad Sci USA. 2000;97:6640-5.

89 6. Miller JH. A short course in bacterial genetics: a laboratory manual and handbook for
90 *Escherichia coli* and related bacteria. Cold Spring Harbor: Cold Spring Harbor Laboratory Press;
91 1992 1992.

92 7. Foster PL. Methods for determining spontaneous mutation rates. Methods Enzymol.
93 2006;409:195-213.

94 8. Hall BM, Ma CX, Liang P, Singh KK. Fluctuation analysis CalculatOR: a web tool for the
95 determination of mutation rate using Luria-Delbruck fluctuation analysis. Bioinformatics.

96 2009;25(12):1564-5.

- 97 9. Foster PL, Lee H, Popodi E, Townes JP, Tang H. Determinants of spontaneous mutation in
98 the bacterium *Escherichia coli* as revealed by whole-genome sequencing. Proceedings of the
99 National Academy of Sciences of the United States of America. 2015;112(44):E5990-E599.
- 100 10. Foster PL, Niccum BA, Popodi E, Townes JP, Lee H, MohammedIsmail W, et al.
101 Determinants of base-pair substitution patterns revealed by whole-genome sequencing of DNA
102 mismatch repair defective *Escherichia coli*. Genetics. 2018;209(4):1029-42.
- 103 11. Li H, Durbin R. Fast and accurate short read alignment with Burrows-Wheeler transform.
104 Bioinformatics. 2009;25(14):1754-60.
- 105 12. Wang X, Lesterlin C, Reyes-Lamothe R, Ball G, Sherratt DJ. Replication and segregation of
106 an *Escherichia coli* chromosome with two replication origins. Proceedings of the National
107 Academy of Sciences of the United States of America. 2011;108(26):E243-50.
- 108 13. Niccum BA, Lee H, MohammedIsmail W, Tang H, Foster PL. The spectrum of replication
109 errors in the absence of error correction assayed across the whole genome of *Escherichia coli*.
110 Genetics. 2018;209(4):1043-54.
- 111 14. Blank K, Hensel M, Gerlach RG. Rapid and highly efficient method for scarless
112 mutagenesis within the *Salmonella enterica* chromosome. PLoS One. 2011;6(1):e15763.

113

114

115 **Supplementary Figure Legends**

116 **Supplementary Figure S1.** The BPS density pattern is not due to transcription but is affected by
117 moving the origin of replication. Shown are plots of the wavelet coherence between two
118 binned BPS data sets. The colors give the magnitude-squared coherence, a measure of the
119 correlation between the data sets, according to the scale on the left. The dotted line gives the
120 “cone of influence” within which the results are free of artifactual edge effects. Arrows indicate
121 the phase-lag between the two data sets; arrows pointing right indicate in-phase, arrows
122 pointing left indicate 180° out-of-phase, and arrows pointing in other directions indicate the
123 various degrees in between. **Supplementary Figure S1A.** The wavelet coherence between the
124 binned BPS data from the MMR-defective strains taken in the clockwise and counterclockwise
125 directions around the chromosome. This presentation illustrates the almost complete
126 symmetry of the BPS density pattern. **Supplementary Figure S1B.** Plot of the wavelet coherence
127 between the BPS data from the MMR-defective strains and the mean binned reads from RNA-
128 Seq samples taken during lag, log, and stationary growth phases of the *ΔmutL* mutant strain,
129 PFM144. **Supplementary Figures S1C, D, E, and F.** Plots of the wavelet coherence between the
130 binned BPS data from the MMR-defective strains and the indicated mutant strains. See text for
131 a description of the strains. Strains: S1C, PFM421; S1D, PFM430/431; S1E, PFM426; S1F,
132 PFM533/534.

133 **Supplementary Figure S2.** Altering the progression of DNA replication affects the BPS density
134 pattern. Plots of the wavelet coherence between the binned BPS data from the MMR-defective
135 strains and the indicated mutant strains. The colors give the magnitude-squared coherence, a
136 measure of the correlation between the data sets, according to the scale on the left. The dotted

137 line gives the “cone of influence” within which the results are free of artifactual edge effects.

138 Arrows indicate the phase-lag between the two data sets; arrows pointing right indicate in-

139 phase, arrows pointing left indicate 180° out-of-phase, and arrows pointing in other directions

140 indicate the various degrees in between. **Supplementary Figures S2A, B, C, and D.** Altering the

141 cellular growth rate by growing a $\Delta mutS$ mutant strain on different medium and at different

142 temperatures differentially affects the BPS density pattern. In the experiments shown in Plot A,

143 C, and D, the cells grew at about half the normal rate, whereas in the experiment shown in plot

144 B they grew at the normal rate. Strains: S2A, B, and C, PFM343; S2D, PFM342. **Supplementary**

145 **Figures S2E and F.** Dysregulation of dNTP levels and loss of Rep, the auxiliary replication

146 helicase, affect the BPS density pattern. Strains: S2E, PFM799; S2F, PFM677. **Supplementary**

147 **Figures S2G and H.** Loss of the Tus antihelicase has no effect, but loss of the terminus

148 organizing protein, MatP, changes the BPS density pattern across the chromosome. Strains:

149 S2G, PFM256; S2H, PFM257.

150 **Supplementary Figure S3.** Loss of RecA, HU α , or Fis changes the BPS pattern, but the SOS

151 response and other NAPs do not. For a description of the plots, see the legend to

152 Supplementary Figure S2. **Supplementary Figures S3A, B, and C.** Loss of RecA alters the BPS

153 density pattern in the terminus region, but not through its role as a master regulator of the SOS

154 response. RecA (Figure S3A) is *E. coli*'s major recombinase. The *umuDC* and *dinB* genes (Figure

155 S3B) encode error-prone DNA polymerases that are induced as part of the SOS response. The

156 *lexA3* allele encodes a non-inducible repressor of the SOS genes. Deletion of *suIA* prevents

157 lethal filamentation, which is not relevant to this study. Strains: S3A, PFM422; S3B, PFM118;

158 S3C, PFM120. **Supplementary Figures S3D, E, F, G, and H.** Loss of the HU α subunit of HU or of

159 Fis changes the BPS density pattern, but loss of the HU β subunit of HU, HNS, or DPS have only
160 minor effects. Strains: S3D, PFM259; S3E, PFM258; S3F, PFM317/318; S3G, PFM741/742; S3H,
161 PFM713.

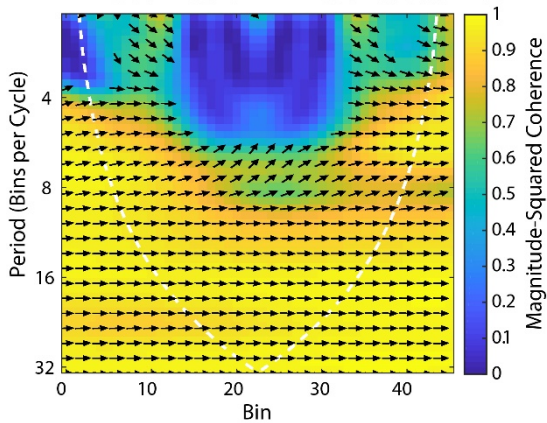
162 **Supplementary Figure S4.** The BPS density pattern is a result of biased correction by replication
163 proofreading and MMR. For a description of the plots, see the legend to Supplementary Figure
164 S2. **Supplementary Figures S4A and B.** A strain with deficient proofreading but active MMR
165 yields a BPS pattern similar to a MMR-defective strain, but a strain with neither proofreading
166 nor MMR does not. The *mutD5* allele encodes an exonuclease-deficient proofreader. Strains:
167 S4A, PFM163; S4B, PFM165/397/399. **Supplementary Figures S4C and D.** The BPS density
168 pattern in the wild-type strain does not match the pattern of either the MMR-defective strain,
169 or the *mutD5* mutant strain. Strains: S4C and D, eight strains with wild-type mutational
170 phenotypes (see text). **Supplementary Figures S4E and F.** MMR-defective *B. subtilis* also has a
171 symmetrical BPS density pattern, but it is different than *E. coli*'s pattern. Strains: three *B.*
172 *subtilis* mutant strains with the same mutational phenotype (see Supplemental Tables S1 and
173 S3).

174 **Supplementary Figure S5:** The BPS density patterns from experiments mentioned in the text
175 but not shown. For each plot the data were collected into 100 Kb bins starting at the origin of
176 replication on the left and continuing around the chromosome back to the origin. The BPS
177 density patterns (bars) and Daubechies wavelet transforms (pink lines) of the indicated strains
178 are compared to the Daubechies wavelet transform of the combined MMR⁻ strains (grey line).
179 In each plot the left-hand scale has been adjusted to bring the wavelets close together for

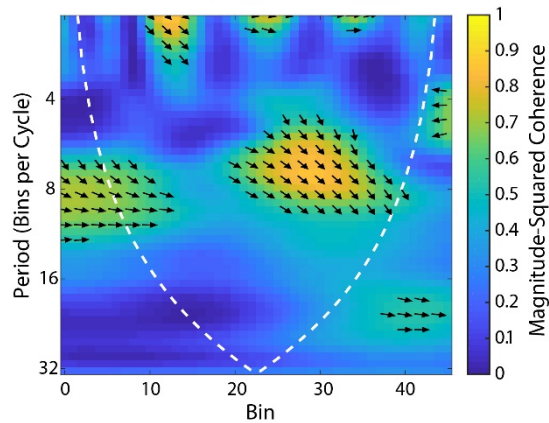
180 comparison. Strains: S5A, MMR strains but A:T transitions at 5'NAC3'/3'NTG5' sites removed;
181 S5B, PFM669; S5C, PFM5; S5D, PFM424; S5E, PFM456; S5F, PFM482.
182 **Supplementary Figure S6:** Plots of the wavelet coherence between the binned BPS data from
183 the MMR-defective strains and the data from the experiments shown in Supplementary Figure
184 S5. See the legends from Supplementary Figure S2 and S5 for details

Supplementary Figure S1

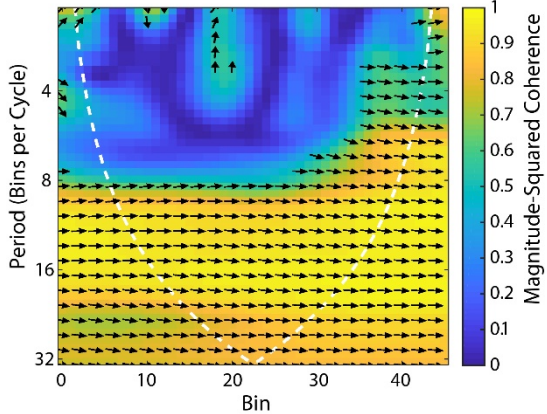
A MMR⁻ Clockwise vs MMR⁻ Counterclockwise



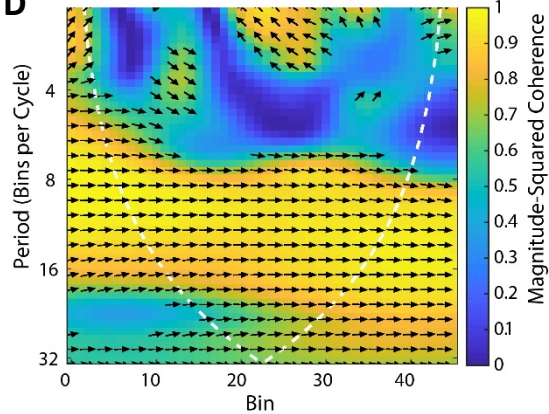
B MMR⁻ vs Mean RNA Reads



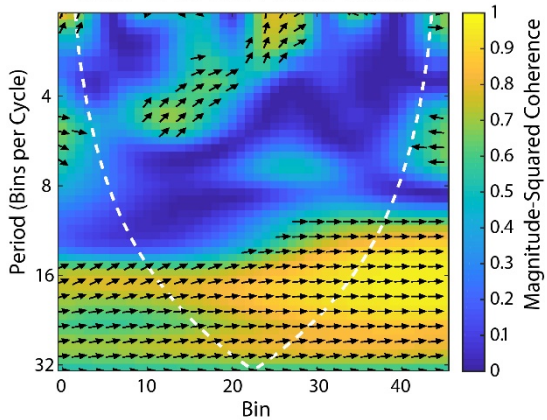
C MMR⁻ vs $\Delta rnhA$



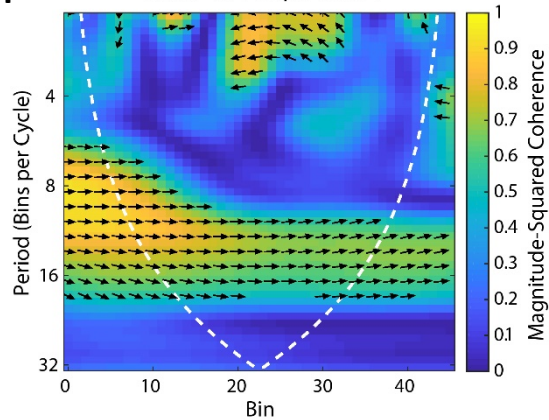
D MMR⁻ vs AB1157 $\Delta mutL oriC^+ oriZ^+$



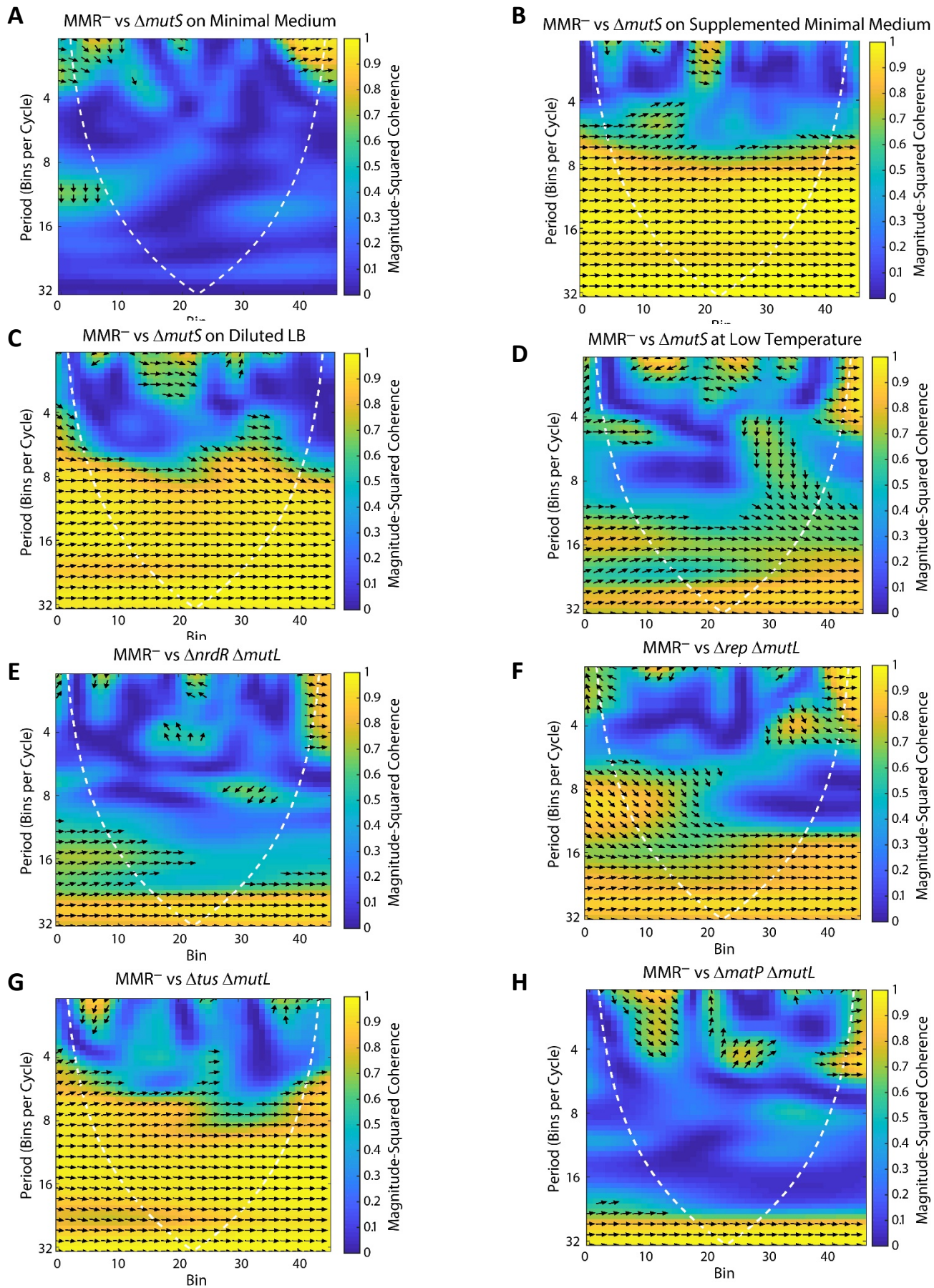
E MMR⁻ vs AB1157 $\Delta mutL \Delta oriC oriZ^+$



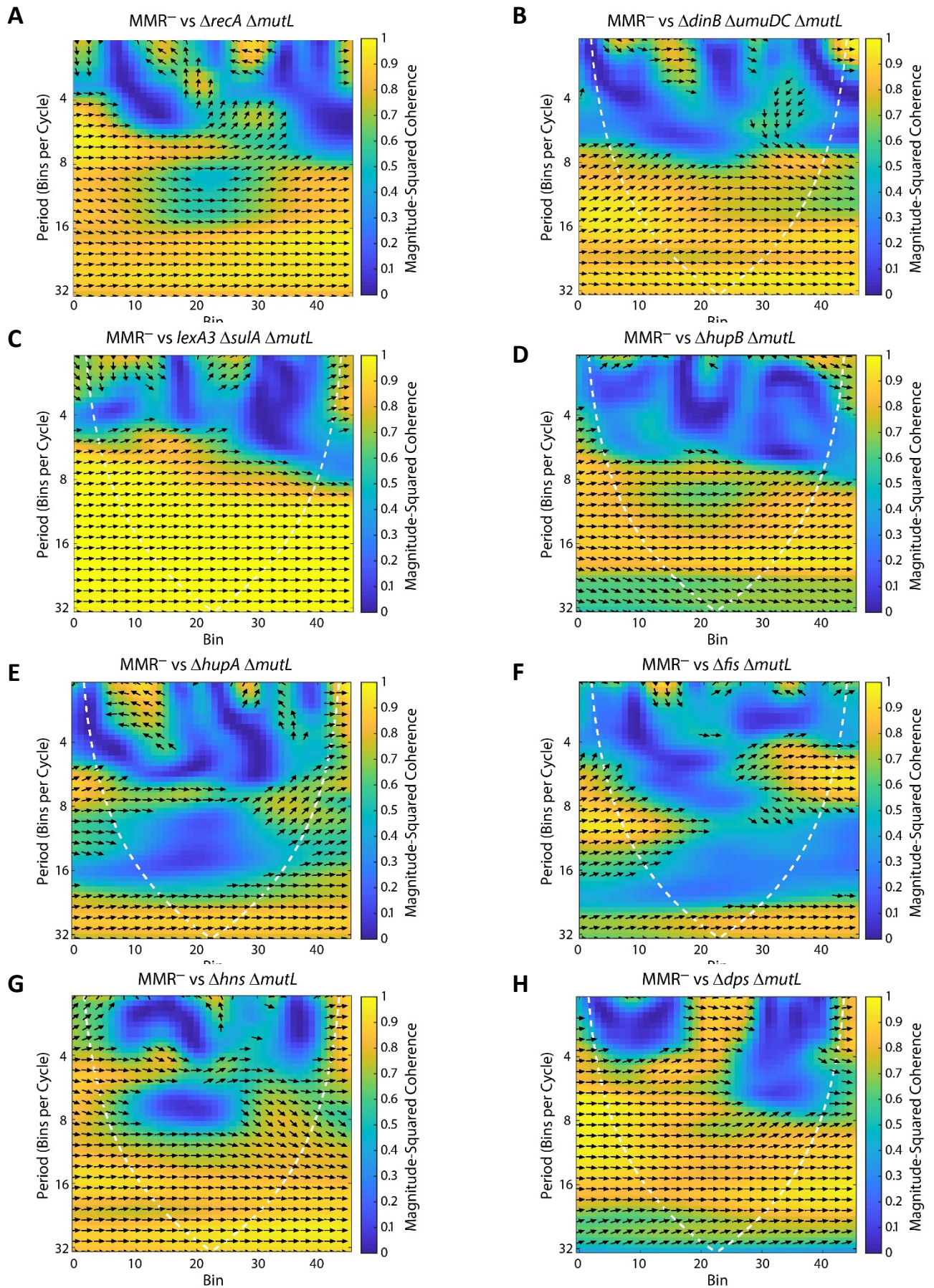
F MMR⁻ vs $\Delta seqA \Delta mutL$



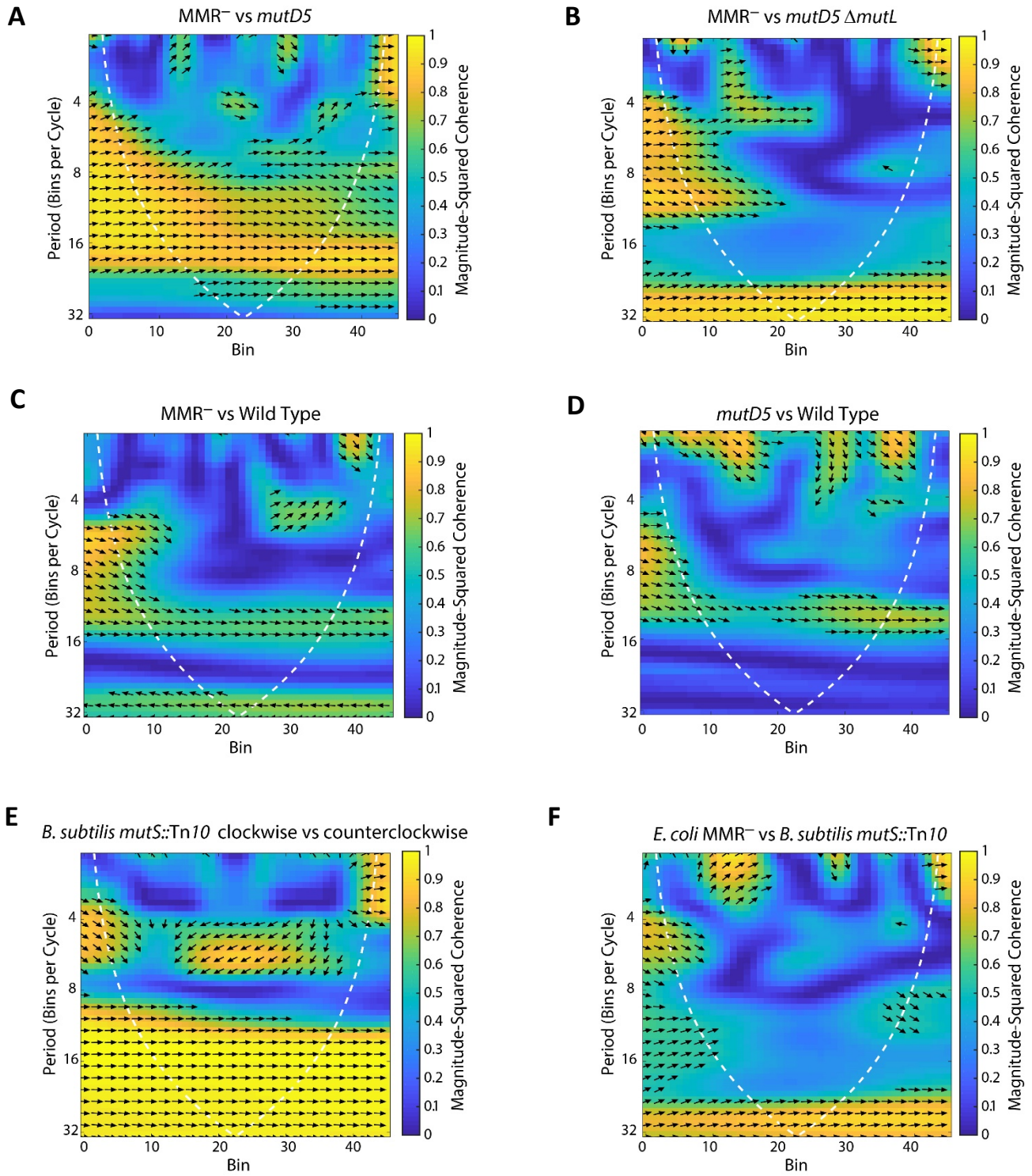
Supplementary Figure S2



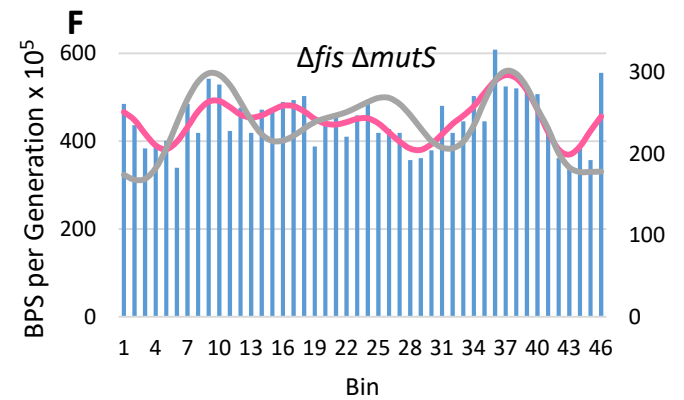
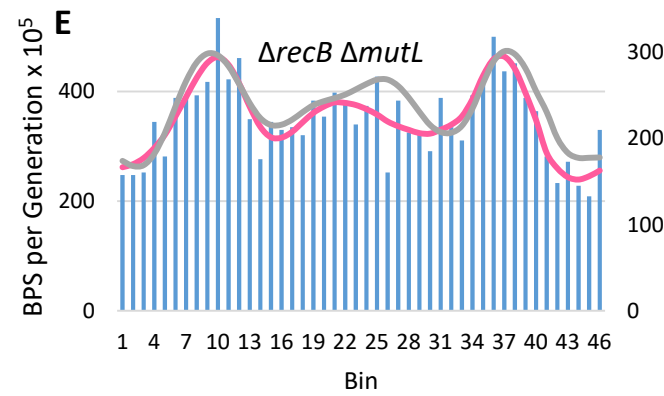
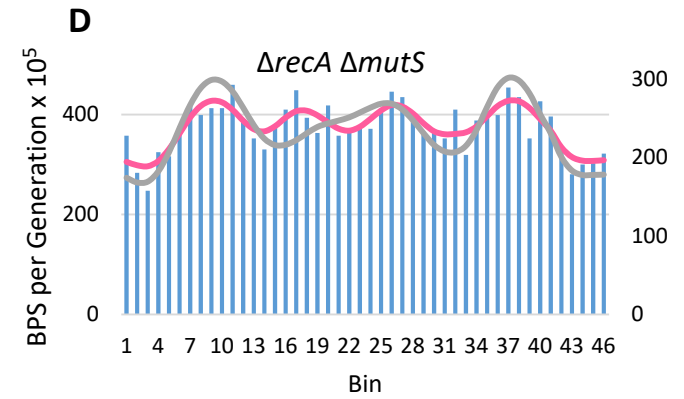
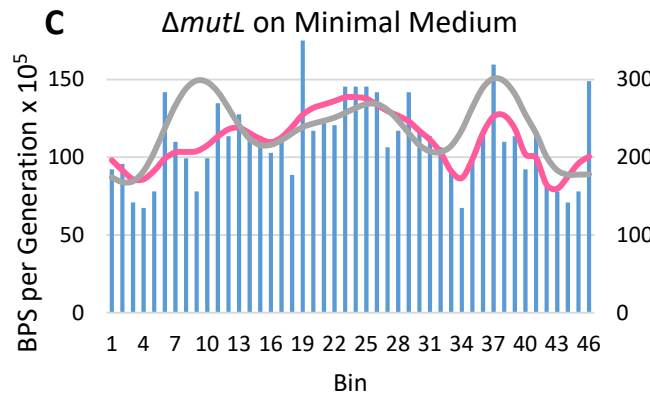
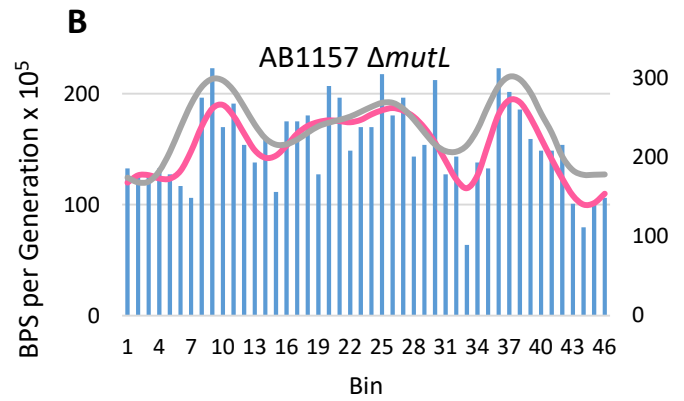
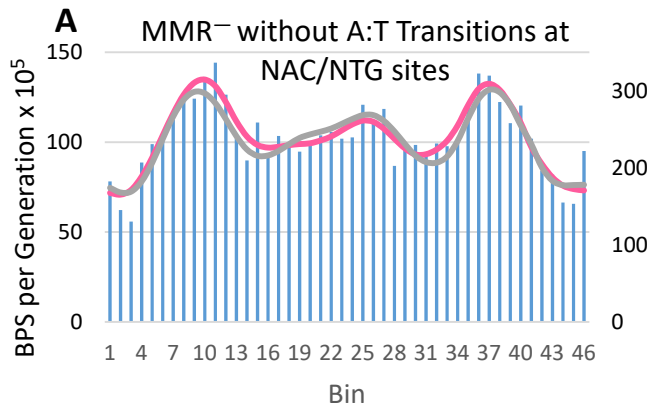
Supplementary Figure S3



Supplementary Figure S4



Supplementary Figure S5



Supplementary Figure S6

